Spin flips in generic black hole binaries

Carlos O. Lousto, James Healy, and Hiroyuki Nakano

Phys. Rev. D **93**, 044031 — Published 10 February 2016

DOI: 10.1103/PhysRevD.93.044031

Spin flips in generic black hole binaries

Carlos O. Lousto,[1] James Healy,[1] and Hiroyuki Nakano[1,2]

[1] *Center for Computational Relativity and Gravitation, School of Mathematical Sciences, Rochester Institute of Technology, 85 Lomb Memorial Drive, Rochester, New York 14623*

[2] *Department of Physics, Kyoto University, Kyoto 606-8502, Japan*

We study the spin dynamics of individual black holes in a binary system. In particular we focus on the polar precession of spins and the possibility of a complete flip of spins with respect to the orbital plane. We perform a full numerical simulation that displays these characteristics. We evolve equal mass binary spinning black holes for $t = 20,000M$ from an initial proper separation of $d = 25M$ down to merger after 48.5 orbits. We compute the gravitational radiation from this system and compare it to 3.5 post-Newtonian generated waveforms finding close agreement. We then further use 3.5 post-Newtonian evolutions to show the extension of this spin *flip-flop* phenomenon to unequal mass binaries. We also provide analytic expressions to approximate the maximum *flip-flop* angle and frequency in terms of the binary spins and mass ratio parameters at a given orbital radius. Finally we discuss the effect this spin *flip-flop* would have on accreting matter and other potential observational effects.

PACS numbers: 04.25.dg, 04.25.Nx, 04.30.Db, 04.70.Bw

I. INTRODUCTION

In this first decade since the breakthroughs [1–3] that allowed to numerically solve General Relativity's field equations for the evolution of black hole binaries (BHB), we have gained many new insights on these systems. The computation of theoretical gravitational waveforms from these BHB systems is very important for first detection and estimation of binary's parameters [4–7]. It is also of astrophysical interest to study the BHB orbital and spin dynamics in precessing systems and how accreting matter interacts with them.

The spin of each individual black hole (BH) can notably affect its orbital motion as displayed, for instance, by the *hangup* mechanism [8], which delays or prompts the merger of the binary according to the sign of the spin-orbit coupling, thus ensuring the formation of a *horizon* (cosmic censorship hypothesis) at merger before the final hole settles to a Kerr BH [9, 10] (no hair theorem).

One of the most notable predictions of numerical relativity is that the remnant of the merger of two highly spinning BHs may receive a recoil of thousands of km/s [11–13] due to asymmetrical emission of gravitational radiation induced by the BH spins [14, 15]. This developed intense astronomical searches for such fast moving BHs that may completely escape from their host galaxies or produce observable disturbances to the velocity field of stars in their cores [16].

New developments in numerical relativity allowed the study of relatively far separated binaries, up to distances of $100M$ in Ref. [17], and mass ratios of $100:1$ in Refs. [18, 19]. Very long term evolutions are now possible [20, 21] as well as the study of near maximally spinning BHBs [22–24].

In Ref. [20], we have found that the spin of BHs can completely reverse sign during its orbital stage. This *flip-flop* of spins is due to a spin-spin coupling effect and may have important observational consequences when the binary system is accreting gas from a galactic environment [25]. In this paper we extend the analysis to unequal mass binaries using 3.5 post-Newtonian (PN) evolutions. Those proved a reliable description for this scenario when compared to the long term full numerical simulation of an equal mass binary [20].

This paper is organized as follows. In Sec. II we revisit the equal mass binary scenario providing further detail and analysis of our full numerical simulation. We also provide a simple vector analysis to understand the mechanism behind the *flip-flop* and then a 2PN analytic study to describe its spin dynamics. In Sec. III we study the case of unequal mass binaries. We use 3.5PN evolutions of the equations of motion coupled with the 2PN spin dynamics to find the configurations that maximize the *flip-flop* angle and the likelihood of a *flip-flop* angle to occur given plausible astrophysical distribution of binary parameters. We also provide 2PN analytic expressions to approximate the *flip-flop* angle and frequency as measured in the orbital frame and asymptotic frame described in terms of projections with respect to the orbital angular momentum $\vec{L}$ and total angular momentum $\vec{J}$. We end the paper with Sec. IV where we make some estimates of the effect this *flip-flop* phenomena could have in realistic astrophysical scenarios and suggest that detailed simulations involving the magnetohydrodynamical description of accreting matter onto BHs are needed to find the characteristic electromagnetic signatures of the *flip-flop*. The appendix A provides details on the PN computation of the flip-flop frequencies and angles.

II. EQUAL MASSES BINARIES

We first study the case of equal mass binaries since they cleanly display the flip-flop effect on the spins of

TABLE I. Initial data parameters and system details. The punctures are located at $\vec{r}_1 = (x_1, 0, z)$ and $\vec{r}_2 = (x_2, 0, z)$, with momenta $\vec{P} = \pm(0, P, 0)$, spins $\vec{S}_1 = (0, 0, S_{1z})$ and $\vec{S}_2 = (S_{2x}, 0, S_{2z})$, mass parameters m^p, horizon (Christodoulou) masses m^H, total ADM mass $M_{\rm ADM}$, and dimensionless spins $\alpha = a/m_H = S/m_H^2$. The horizon masses and spins are given after the gauge settles, and the errors in those quantities, denoted as δm^H and $\delta\alpha$, are determined by the drift in the quantity during the inspiral. Also provided are the simple proper distance d, eccentricity at the start of the inspiral e_i, and eccentricity e_f and the number of orbits N just before merger.

x_1/m	x_2/m	z/m	P/m	d/m
10.73983	-10.76016	-0.01968	0.05909	25.37
m_1^p/m	m_2^p/m	S_{1z}/m^2	S_{2x}/m^2	S_{2z}/m^2
0.48543	0.30697	0.05	0.19365	-0.05
$M_{\rm ADM}/m$	$J_{\rm ADM}/m^2$	e_i	e_f	N
0.99472	1.2704344	0.0322	0.0006	48.5
m_1^H/m	$\delta m_1^H/m$	m_2^H/m	$\delta m_2^H/m$	
0.50000	0.00002	0.49974	0.00001	
α_1	$\delta\alpha_1$	α_2	$\delta\alpha_2$	
0.20003	0.00056	0.80088	0.00066	

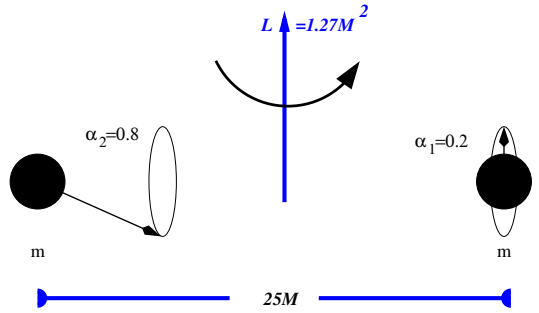

FIG. 1. Initial configuration of the simulated binary.

the holes and allow for a simple approximate analytic model of the process. In Sec. III we will study in detail its mass ratio dependence.

A. Full Numerical Evolution

In order to verify the realization of the spin flip-flops in the presence of gravitational radiation and the full non-linearities of General Relativity during the final stages of the inspiral, we consider a long-term full numerical simulation with initial configuration as described in Table I and depicted in Fig. 1.

We evolve the following BHB data sets using the LazEv [26] implementation of the moving puncture approach [2, 3] with the conformal function $W = \sqrt{\chi} = \exp(-2\phi)$ suggested by Ref. [27]. For the run presented here, we use centered, eighth-order finite differencing in space [28] and a fourth-order Runge Kutta time integrator (note that we do not upwind the advection terms).

Our code uses the EinsteinToolkit [29, 30] / Cactus [31] / Carpet [32] infrastructure. The Carpet mesh refinement driver provides a "moving boxes" style of mesh refinement. In this approach, refined grids of fixed size are arranged about the coordinate centers of both holes. The Carpet code then moves these fine grids about the computational domain by following the trajectories of the two BHs.

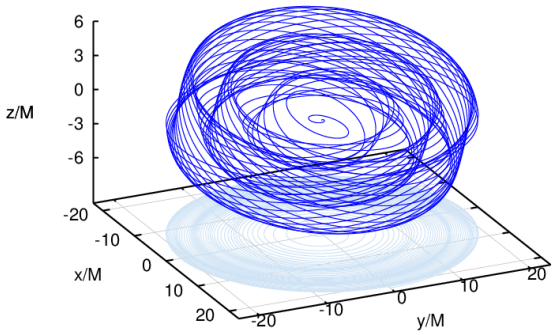

FIG. 2. Precession of the orbital plane as displayed by the distance vector $\vec{d} = \vec{x}_1(t) - \vec{x}_2(t)$.

We use AHFinderDirect [33] to locate apparent horizons. We measure the magnitude of the horizon spin using the *isolated horizon* (IH) algorithm detailed in Ref. [34] and as implemented in Ref. [35]. Note that once we have the horizon spin, we can calculate the horizon mass via the Christodoulou formula

$$m_H = \sqrt{m_{\rm irr}^2 + S_H^2/(4m_{\rm irr}^2)}\,, \qquad (1)$$

where $m_{\rm irr} = \sqrt{A/(16\pi)}$, A is the surface area of the horizon, and S_H is the spin angular momentum of the BH (in units of M^2). In the tables below, we use the variation in the measured horizon irreducible mass and spin during the simulation as a measure of the error in computing these quantities. We measure radiated energy, linear momentum, and angular momentum, in terms of the radiative Weyl Scalar ψ_4, using the formulas provided in Refs. [36, 37]. However, rather than using the full ψ_4, we decompose it into ℓ and m modes and solve for the radiated linear momentum, dropping terms with $\ell > 6$. The formulas in Refs. [36, 37] are valid at $r = \infty$. We extract the radiated energy-momentum at finite radius and extrapolate to $r = \infty$, and find that the new perturbative extrapolation described in Ref. [38] provides the most accurate waveforms. While the difference of fitting both linear and quadratic extrapolations provides an independent measure of the error.

Figure 2 highlights the important effects of precession of the orbital plane during the whole evolution and the three precession cycles occurring over the nearly 50 orbits.

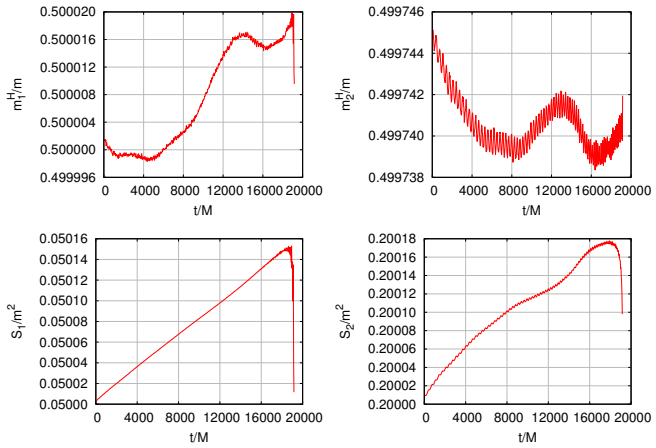

FIG. 3. The conservation of the individual masses and spin magnitudes of the holes during the binary evolution.

Through evolution we track the horizon mass and magnitude and components of the individual spins of the BHs. Figure 3 displays the levels at which these quantities are conserved during the $t = 20,000M$ of full numerical evolution and this provides a measure of the accuracy of the simulation, i.e., the variations in $\Delta m_1^H/m_1^H \approx 4\times10^{-5}$, $\Delta S_1^H/S_1^H \approx 3\times10^{-3}$, $\Delta m_2^H/m_2^H \approx 1.2\times10^{-5}$, and $\Delta S_2^H/S_2^H \approx 9\times10^{-4}$.

The spin components in the simulation coordinate system are displayed in Fig. 4. They show the polar component of $\vec{S}_1$ from alignment at $t = 0$ to almost misalignment at merger and the complementary behavior for $\vec{S}_2$. From the variations with time of the $(\hat{x}, \hat{y})$ components of the spins one can also read-off the precessional effects. While these are coordinate based periods, one can verify, for instance from the oscillations in the amplitude of the $(\ell = 2, m = 1)$ mode of the gravitational waveform in a gauge invariant way that those periods correspond to the physical dynamics of spins (see Fig. 6 in this paper and also Ref. [39]).

Another useful representation of the spins [20] is given in Fig. 5 where the flip-flopping spin's $(\hat{S}_1)$ trajectory can be described as a composition of the polar (flip-flop) and azimuthal (precession) dynamics which resembles that of an orange peeling. For the sake of future interpretations and applications we also provide the spin trajectories as seen in an (approximately) inertial frame where the direction of the total angular momentum $\hat{J}$ is conserved and coincident (approximately) with the coordinate direction $\hat{z}$.

The gravitational waveforms from spinning, precessing BHB systems are of great interest for detection and parameter estimation in the forthcoming observation of gravitational waves by Advanced LIGO [40] and other laser interferometric gravitational wave observatories. Our simulation produced one of the longest waveforms studied to date, starting from an initial configuration with proper separation, $d = 25M$. This is well in

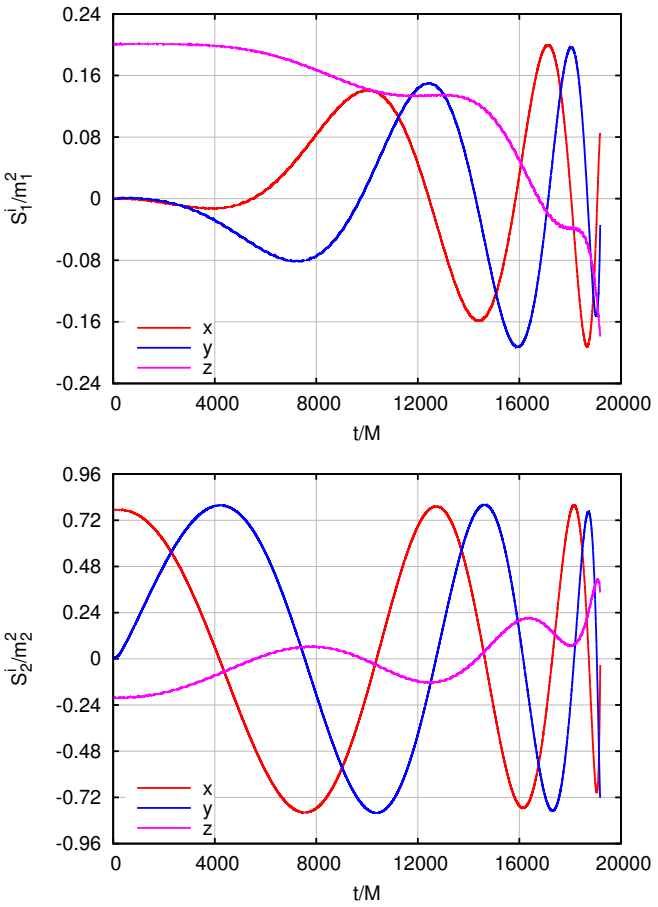

FIG. 4. BH (1,2) spin components in the coordinate frame. The top panel is BH1 and the bottom panel is BH2.

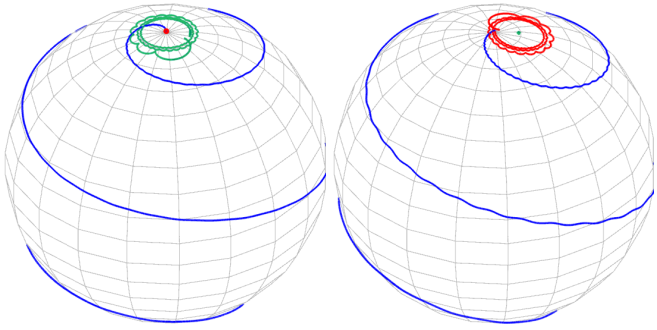

FIG. 5. Change in the spin direction (in blue) of the BH1 (with the smaller spin magnitude) in the orbital frame, $\hat{L}$ (left), and the coordinate frame $\hat{z}$ (right). Plotted also the directions of $\vec{L}$ in red and $\vec{J}$ in green.

the post-Newtonian regime (see also the recent simulation [21] for nonspinning, unequal mass binaries starting at an initial separation $d = 27M$). In Fig. 6 the leading modes $(\ell = 2, m = 2)$ and (2, 1) are displayed [20] and the first shows the well known chirp behavior with essentially monotonic increase of amplitude and frequency until merger. The second waveform, corresponding to the

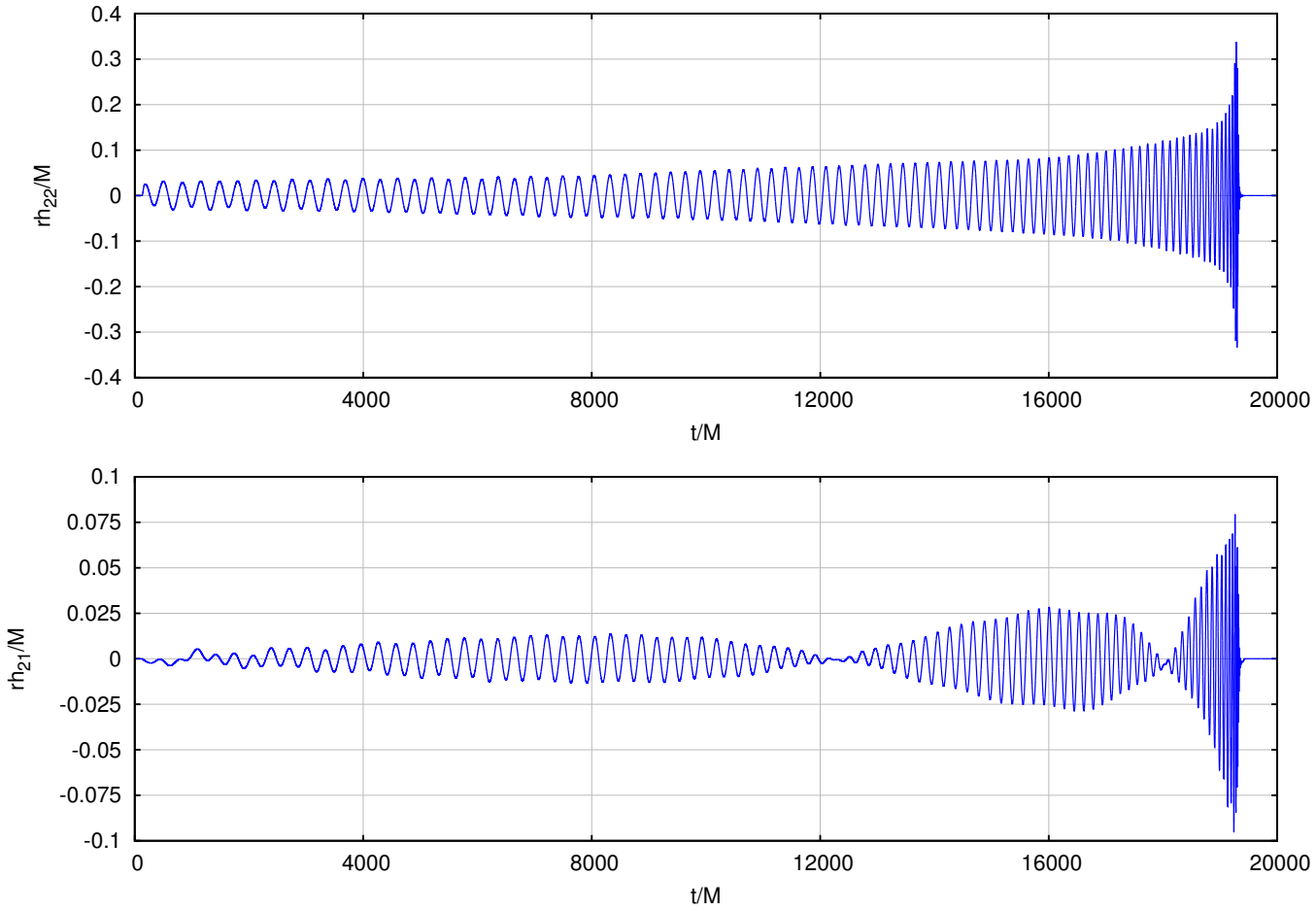

FIG. 6. The full numerical ($\ell = 2$, $m = 2$) waveform (above) and ($\ell = 2$, $m = 1$) waveform (below) as extracted by observers at $r = 175M$.

($\ell = 2$, $m = 1$) mode, displays a modulation in amplitude that corresponds to the period of precession of the orbital plane (and in this equal mass binary case this is coincident with the precession of the spins). Thus this waveform provides an independent and gauge invariant measure of the precession period.

Of particular interest is to determine the precision of this waveform. Due to the high computational demand of this simulation, 2.5 million service units on 25 to 30 nodes of our local cluster "Blue Sky" with dual Intel Xeon E5-2680 processors nearing $100M$ of evolution per day, we have not produced detailed convergence studies involving several runs at different resolutions. Instead we compare our full numerical waveforms with those produced with 3.5PN evolutions and found excellent agreement, particularly at early times, when 3.5PN is expected to be very accurate, given the large initial separation of the holes.

Figures 7 and 8 display the differences of the numerical and PN waveform for the ($\ell = 2, m = 2$) mode phase and amplitude, respectively. Since the full numerical waveforms are extracted at a finite observer location (in this case at $r = 175M$) we extrapolate them to null infinity with a recent $\mathcal{O}(1/r^2)$ accurate perturbative method [38, 41] to obtain further agreement, showing reasonable errors until near the final merger.

Since this BHB simulation is relatively long-term it is well suited to study the evolution of the eccentricity as a function of the binary's separation. Using the method of Ref. [42] to determine e_D, we measure the eccentricity per orbit (we have not included the first two orbits, contaminated by gauge settling, and last few orbits due to strong radiative effects). As the binary's separation shrinks due to gravitational radiation the eccentricity reduces as shown in Fig. 9. We performed a fit to the measured eccentricity versus separation of the form $a\, r^b$ obtaining an exponent $b = 1.73486 \pm 0.1495$ to compare with the lowest post-Newtonian prediction of Ref. [43] for radiation of eccentricity, $e \sim r^{19/12}$. With $19/12 = 1.5833$,

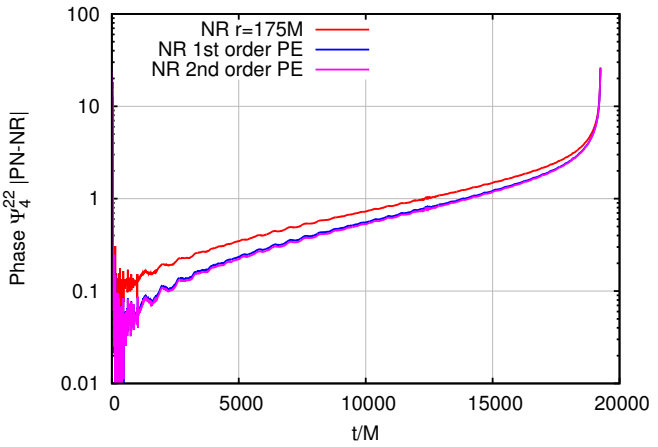

FIG. 7. The phase difference between the full numerically generated ($\ell = 2, m = 2$) waveform (NR) and the 3.5PN waveform. Differences are notably reduced when the NR-waveform, extracted at $r = 175M$, is extrapolated to an infinite observer location by the perturbative formulae (PE) of 1st order, accurate to $(1/r)$ terms and second order, accurate to $(1/r^2)$.

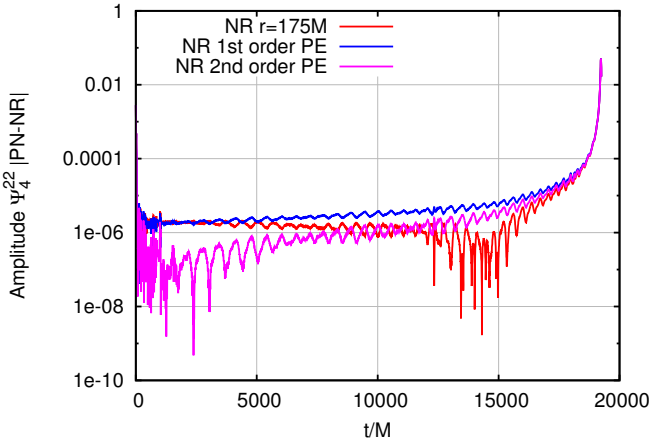

FIG. 8. The amplitude difference between the full numerically generated ($\ell = 2, m = 2$) waveform (NR) and the 3.5PN waveform. Differences are notably reduced when the NR-waveform, extracted at $r = 175M$, is extrapolated to an infinite observer location by the perturbative formulae (PE) of 1st order, $(1/r)$, and second order, $(1/r^2)$.

the post-Newtonian prediction is within the statistical error bars of the fit.

After merger the binary forms a single final remnant BH with characteristics given in Table II. Notably the recoil velocity reaches 1500 km/s in agreement with the empirical predictions [15, 44].

Figure 10 displays the settling of the final mass and spin measures as the final BH radiates away its last distortions and becomes a quiet Kerr BH [9].

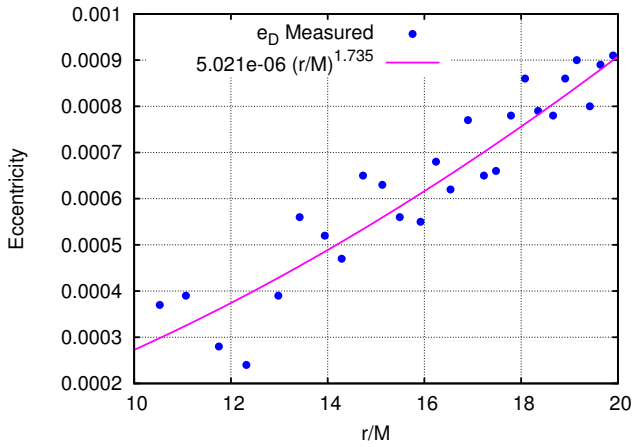

FIG. 9. Evolution of the eccentricity versus coordinate separation of the BHB. Dots represent measurements of the eccentricity, e_D, and the continuous curve a fit to its decay with $e \sim r^{1.73486 \pm 0.1495}$. In comparison, the theoretical prediction is $e \sim r^{1.5833}$.

TABLE II. Remnant properties and recoil velocity. The final mass and spin are measured from the horizon, and the recoil velocity is calculated from the gravitational waveforms. The error in the mass and spin is determined by the drift in those quantities after the remnant settles down. The error in the recoil velocity is estimated by the difference between first and second order polynomial extrapolation to infinity of the waveforms.

M_{rem}/m	$\lvert\alpha_{rem}\rvert$	V_{recoil} [km/s]
0.94904 ± 0.00000	0.70377 ± 0.00002	1508.49 ± 16.08
α^x_{rem}	α^y_{rem}	α^z_{rem}
0.10815 ± 0.00003	-0.01986 ± 0.00000	0.69513 ± 0.00002

B. Vector Analysis

In order to visualize the origin of this flip-flop effect we can use a simple vector addition model to represent the total angular momentum of the system, $\vec{J} = \vec{L} + \vec{S}$, as the sum of the orbital angular momentum $\vec{L}$ and the total spin $\vec{S} = \vec{S}_1 + \vec{S}_2$. This total spin being the sum of the individual spin of the holes $\vec{S}_1$ and $\vec{S}_2$ as represented in Fig. 11.

In this picture, the six degrees of freedom of the spins $\vec{S}_1$ and $\vec{S}_2$ are shown as vectors in 3-space. These de-

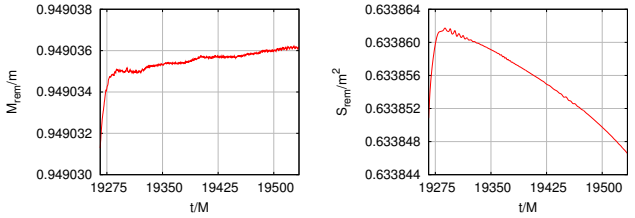

FIG. 10. The mass and spin of the final merged BH.

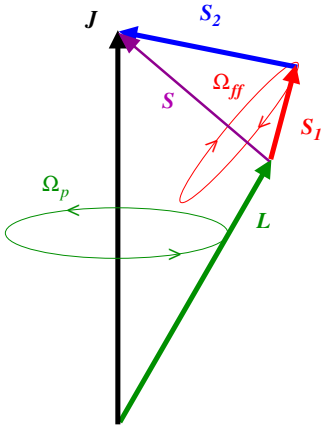

FIG. 11. Flip-flop of $\vec{S}_1$ and $\vec{S}_2$ as they precess with $\vec{L}$.

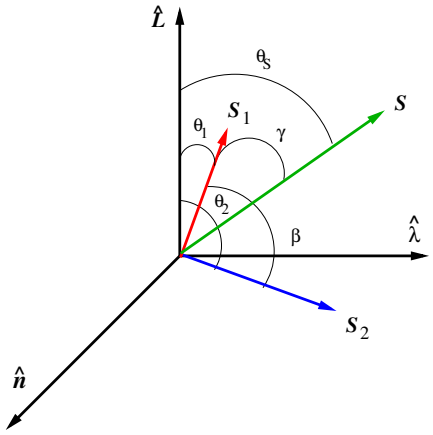

FIG. 12. The configuration of the spins in the orbiting frame. Spin configurations $\vec{S}_1$ and $\vec{S}_2$ relative to the orbital angular momentum $\vec{L}$. Here $\vec{S} = \vec{S}_1 + \vec{S}_2$.

grees of freedom are constrained by the conservation of the magnitude of the individual spins S_1, and S_2, the magnitude of the total spin S, and its projection along the orbital angular momentum, $\vec{S}\cdot\hat{L}$. The conservation of the magnitudes of the individual spins and the magnitude of their sum S, can be seen in the 2PN evolution of the spins in Eqs. (7) of Sec. II C. The conservation of $\vec{S}_0\cdot\hat{L}$ was shown in Ref. [45] using the orbit averaged version of Eqs. (7). The conservation of these quantities in full numerical simulations of BHBs has been observed to be approximately true in Refs. [46] and [47]. Note that in what follows to determine the flip-flop angle, we do not use the PN (or full numerical) dynamics beyond the referred conservation of the individual and total spin magnitudes.

It follows hence that the following quantities are conserved (see Fig. 12)

$$\begin{aligned}
\vec{S}\cdot\vec{S} &= S^2 = S_1^2 + S_2^2 + 2S_1S_2\cos\beta = \text{constant}\,,\\
\vec{S}\cdot\vec{S}_1 &= SS_1\cos\gamma = S_1^2 + S_2S_1\cos\beta = \text{constant}\,,\\
\vec{S}\cdot\vec{S}_2 &= SS_2\cos(\beta-\gamma) = S_2^2 + S_2S_1\cos\beta\\
&= \text{constant}\,.
\end{aligned} \tag{2}$$

This leads to the conservation of β and γ during the evolution of the binary.

In particular we find that $\vec{S}_1$ oscillates around $\vec{S}$ between angles γ and $-\gamma$ (when it is both coplanar to $\vec{S}$ and $\vec{L}$), where

$$\cos\gamma = \frac{S_1 + S_2\cos\beta}{\sqrt{S_1^2+S_2^2+2S_1S_2\cos\beta}} = \frac{S^2+S_1^2-S_2^2}{2SS_1}\,. \tag{3}$$

BH2 also oscillates at the same flip-flop frequency Ω_{ff}, but with a smaller angle (since we consider $S_2 > S_1$) given by $\pm(\beta-\gamma)$ where

$$\cos(\beta-\gamma) = \frac{S^2+S_2^2-S_1^2}{2SS_2}\,. \tag{4}$$

Thus both spins, $\vec{S}_1$ and $\vec{S}_2$, oscillate around $\vec{S}$ which in turn precesses around $\vec{L}$.

The direction of oscillation of the spins can be seen from the leading precession equation for $d\vec{L}/dt = (7/2r^3)(\vec{J}\times\vec{L})$ indicating that $\vec{L}$ oscillates counterclockwise. Likewise the leading precession for $d\vec{S}_1/dt = (1/r^3)((7/2)\vec{J}\times\vec{S}_1 - 3\vec{S}\times\vec{S}_1)$ indicates that $\vec{S}_1$ oscillates clockwise around $\vec{S}$ (see Eqs. (9) for the precise expression). Thus Fig. 11, is represented as seen by an observer located up (north) with respect to $\vec{J}$ direction.

We can define the flip-flop angle with respect to the polar coordinates as measured from $\hat{L}$ (analogous formulae can be defined for $\hat{J}$)

$$\Delta\theta_i^{ff} = \theta_i^{max} - \theta_i^{min}\,, \tag{5}$$

where $i = 1, 2$ labels either BH spin.

We have three cases to consider depending on θ_S, where $\cos(\theta_S) = S_L/S = (\vec{S}\cdot\hat{L})/S$,

$$\Delta\theta_1^{ff} = \begin{cases} \theta_S + \gamma & \text{if } 0 \le \theta_S \le \gamma\,,\\ 2\gamma & \text{if } \gamma \le \theta_S \le \pi-\gamma\,,\\ \pi - \theta_S + \gamma & \text{if } \pi-\gamma \le \theta_S \le \pi\,, \end{cases} \tag{6}$$

for $0 \le \gamma \le \pi/2$, and similar for BH2, replacing γ by $\beta-\gamma$. When $\pi/2 \le \gamma \le \pi$, we replace $\gamma \leftrightarrow \pi-\gamma$ in the equation above.

Hence, for instance, in order to maximize the flip-flop angle, we can set $\gamma = \pi/2$, which leads to the vanishing of $\cos\gamma$ on the left hand side of the above equation (3), leading to the condition $S_1 + S_2\cos\beta = 0$, for $q = 1$, used in our full numerical configuration, as detailed in Sec. II A.

This oscillation of the spins represent a *genuine* spin-flip in the sense that it is the same object that completely changes its spin orientation. This is different from the simple case where the final remnant spin has flipped direction compared to the spin of one of the individual orbiting BHs [35]. It is also different from a classic analog of the hyperfine transition of an electron in the Hydrogen

atom flipping its spin and leading to the famous 21 cm radio emission. Here the flip also occurs in a conservative set up, with no emission of gravitational waves, and it is compensated by an opposite flop from the other BH.

C. Post-Newtonian Spin Dynamics

The vector analysis is helpful to visualize the angles of flip-flop but in order to determine their rate of oscillation one has to resort to a dynamical computation. In order to provide simple, approximate, expressions we will perform a 2PN (conservative) study.

The precession equations for the spins $\vec{S}_1$ and $\vec{S}_2$ with a mass ratio $q = m_1/m_2$ to leading spin-orbit and spin-spin couplings in the (2PN) post-Newtonian expansion [48] take the form

$$\frac{d\vec{S}_1}{dt} = \frac{1}{r^3}\left[\left(2+\frac{3}{2q}\right)\vec{L} - \vec{S}_2 + \frac{3(\vec{S}_0\cdot\hat{n})}{1+q}\hat{n}\right]\times\vec{S}_1\,,$$
$$\frac{d\vec{S}_2}{dt} = \frac{1}{r^3}\left[\left(2+\frac{3q}{2}\right)\vec{L} - \vec{S}_1 + \frac{3q(\vec{S}_0\cdot\hat{n})}{1+q}\hat{n}\right]\times\vec{S}_2\,, \quad (7)$$

where $\vec{n} = (\vec{r}_1 - \vec{r}_2)/|\vec{r}_1 - \vec{r}_2|$ and

$$\vec{S}_0 = \left(1+\frac{1}{q}\right)\vec{S}_1 + (1+q)\,\vec{S}_2\,. \quad (8)$$

For more details see, for instance, the reviews in Refs. [49, 50]. The averaging of Eqs. (7) over the orbital period gives

$$\begin{aligned}\langle\dot{\vec{S}}_1\rangle &= \frac{1}{r^3}\left(\left(\frac{7}{2}-\frac{3}{2}\frac{S_{\hat{L}}}{\ell}\right)\vec{L}+\frac{1}{2}\vec{S}_2\right)\times\vec{S}_1\\ &= \frac{1}{r^3}\left(\left(\frac{7}{2}-\frac{3}{2}\frac{S_{\hat{L}}}{\ell}\right)\vec{J}-3\vec{S}\right)\times\vec{S}_1\,,\\ \langle\dot{\vec{S}}_2\rangle &= \frac{1}{r^3}\left(\left(\frac{7}{2}-\frac{3}{2}\frac{S_{\hat{L}}}{\ell}\right)\vec{L}+\frac{1}{2}\vec{S}_1\right)\times\vec{S}_2\\ &= \frac{1}{r^3}\left(\left(\frac{7}{2}-\frac{3}{2}\frac{S_{\hat{L}}}{\ell}\right)\vec{J}-3\vec{S}\right)\times\vec{S}_2\,, \end{aligned} \quad (9)$$

where $\ell = |\vec{L}| = qM^{3/2}r^{1/2}/(1+q)^2$ and we have ignored cubic terms of spins in the most right hand side of each equation.

By decomposing the spins along $\hat{L}$ and perpendicular to it with unit vectors $\hat{\lambda}$ and $\hat{n}$, as shown in Fig. 12, in the fashion of Sec. IV.A of Ref. [44], we obtain the spin evolution equations for $q = 1$ as

$$\begin{aligned}\dot{S}_{1\hat{n}} &= S_{1\hat{\lambda}}\left[\frac{v_\lambda}{r}-\frac{7\ell}{2r^3}\left(1+\frac{S_{1\hat{L}}}{\ell}\right)+\frac{S_{2\hat{L}}}{r^3}\right]-\frac{9S_{1\hat{L}}S_{2\hat{\lambda}}}{2r^3}\,,\\ \dot{S}_{1\hat{\lambda}} &= -S_{1\hat{n}}\left[\frac{v_\lambda}{r}-\frac{7\ell}{2r^3}\left(1+\frac{S_{1\hat{L}}}{\ell}\right)+\frac{S_{2\hat{L}}}{r^3}\right]\\ &\quad+\frac{9S_{1\hat{L}}S_{2\hat{n}}}{2r^3}-\frac{3S_{1\hat{L}}S_{\hat{n}}}{r^3}\left(1+\frac{S_{\hat{L}}}{\ell}\right)\,,\\ \dot{S}_{1\hat{L}} &= \frac{9S_{1\hat{n}}S_{2\hat{\lambda}}}{2r^3}-\frac{9S_{1\hat{\lambda}}S_{2\hat{n}}}{2r^3}+\frac{3S_{1\hat{\lambda}}S_{\hat{n}}}{r^3}\left(1+\frac{S_{\hat{L}}}{\ell}\right)\,, \end{aligned} \quad (10)$$

for $\vec{S}_1$ and similar equations for $\vec{S}_2$ by exchanging labels 1 and 2 from Eqs. (7). In the above expression, $v_\lambda = r\Omega_{orb}$ is the tangential velocity of the binary (in a quasicircular orbit, see Eq. (13) for Ω_{orb}), $S_{i\hat{L}} = \vec{S}_i\cdot\hat{L}$, $S_{i\hat{n}} = \vec{S}_i\cdot\hat{n}$, $S_{i\hat{\lambda}} = \vec{S}_i\cdot\hat{\lambda}$ and $S_{\hat{L}} = \vec{S}\cdot\hat{L}$.

We can then obtain equations of the form $d^2(\vec{S}_i\cdot\hat{L})/dt^2 = \Omega_{ff}^2\,\vec{S}_i\cdot\hat{L}+\cdots$ for $i = 1, 2$ and analogously for the perpendicular component of S_i giving Ω_p. From where we can read-off the orbit averaged polar and azimuthal oscillations frequencies of the spin $\vec{S}_i$ (see also Ref. [45] for the equations projected along $\hat{J}$)

$$\Omega_{ff} = 3\frac{S}{r^3}\left[1-\frac{2\,\vec{S}\cdot\hat{L}}{M^{3/2}r^{1/2}}\right]+\cdots, \quad (11)$$

$$\Omega_p = \frac{7\ell}{2r^3}+\frac{2}{r^3}(\vec{S}\cdot\hat{L})+\cdots, \quad (12)$$

that we identify with the flip-flop and precession frequencies respectively. For the sake of completeness and further reference, the orbital frequency of equal mass binaries in quasicircular orbits is given by Ref. [51]

$$M\Omega_{orb} = \left(\frac{M}{r}\right)^{3/2}-\frac{11}{8}\left(\frac{M}{r}\right)^{5/2}+\cdots. \quad (13)$$

In order to verify the accuracy of the above expressions for the flip-flop frequency and angle we performed a series of 3.5PN numerical integrations representing the merger of BHBs from $r = 100M$ down to $r = 5M$ and measured the flip-flop angle and the frequency of oscillation. The results are presented in Figs. 13 and 14 as a color map with the direct integration of the PN equations of motion coupled to the spin evolutions and we superposed a few curve levels based on the above analytic estimates. We observe good agreement among them, in particular for the maximum flip angle described by $\cos\beta = -S_1/S_2$. Fig. 14 displays as a color map the frequency at the start of the evolution, $r = 100M$ where the term $(3S/r^3)$ in Eq. (11) dominates. In this figure, the thin lines are the contours from the measured flip-flop frequency, and the bold lines are the analytic expression given by Eq. (11) for quasicircular orbits at the corresponding r.

D. Statistics

Let us study first the simplest case of conservative precession for equal mass binaries. In Fig. 15, we display the probability of a flip-flop angle $\Delta\theta_{ff} \geq x$ assuming equal masses with random spin orientations and magnitudes of BH1 and 2. For the sake of simplicity, we used here spin evolution equations (7) with no radiation reaction taken into account. The line labeled '2D' considers random angular distribution of one spin and random distribution of the ratio of spin magnitudes. It could represent the scenario where accretion processes succeeded in aligning the spin of one of the BHs, while the spin of the other has still

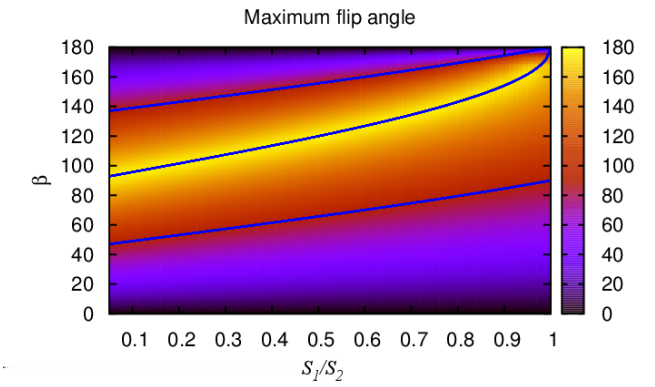

FIG. 13. $q = 1$ binaries, inspiraling from $r = 100M$ to $r = 5M$. Initial configurations having $\phi_1^0 = 0 = \phi_2^0$, $\theta_1^0 = 0$, and varying $\theta_2^0 = \beta$ and S_1/S_2. The central blue curve follows $\cos\beta = -S_2/S_1$ and agrees with the maximum (yellow) of the flip-flop angle of θ_2. The other two blue lines represent the 90-degrees flips level.

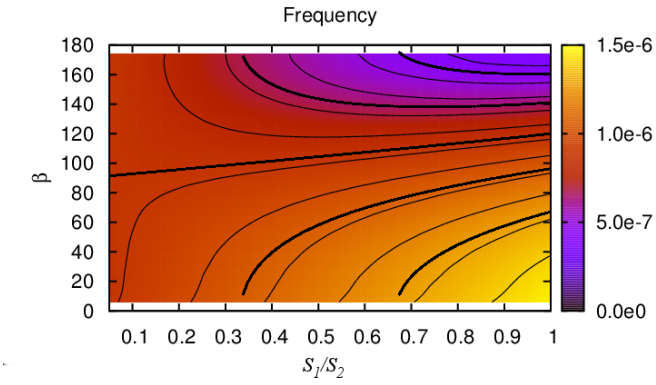

FIG. 14. Flip-flop frequency oscillation for $q = 1$ binaries, inspiraling from $r = 100M$ to $r = 5M$. Starting from initial $\phi_1^0 = 0 = \phi_2^0$, $\theta_1^0 = 0$, for different choices of $\theta_2^0 = \beta$ and S_1/S_2. Different surface levels are represented in units of 10^{-7} for the initial frequency at $r = 100M$. Thin lines are the measured flip-flop frequency during evolution and thick lines their analytic approximation for quasicircular orbits, Eq. (11).

a random orientation due to a much larger time scale for alignment. If we allow instead to vary all six parameters of the BH spins (magnitude and both spin directions) with $q = 1$, we observe the distribution labeled '6D'.

When either BH has its spin aligned or counteraligned with the orbital angular momentum and the other spin is chosen randomly we have a random angle β between the directions of the BH1 and 2 spins. In this case one can obtain from Eq. (3) that the probability of an angle γ given a random distribution of $\cos\beta$ is approximated by

$$P(\cos\gamma) = 1 + \left(\frac{S_1}{S_2}\right)(2\cos\gamma - 1)\,, \tag{14}$$

which upon assuming random distribution of spin magnitudes $0 \leq (S_1/S_2) \leq 1$, leads to the probability for a flip-flop angle larger than x

$$P(\Delta\theta_{ff} > x) = \frac{1}{2}\cos\left(\frac{x}{2}\right)\left(\cos\left(\frac{x}{2}\right) + 1\right)\,. \tag{15}$$

This probability distribution, represented in Fig. 15 by the red continuous curve shows, for instance, that (for equal mass binaries) there is nearly a 60% probability of flip-flops of more than 90°.

In the more general case, allowing for radiation reaction to drive the BHBs towards merger and random variation of all variables, we find the same qualitative behavior as above plus a detailed $\Delta\phi$-dependence. From the expressions for the flip-flop angle in Eq. (6), we observe they depend entirely on the two angles γ and θ_S, both being constants of motion (for equal mass binaries). Thus once we express them in terms of initial data we can predict the flip-flop angle. This can be achieved in terms of four of the six spin components: θ_1, θ_2, $\Delta\phi = \phi_2 - \phi_1$, and S_1/S_2, from Eq. (3) for γ

$$\cos\gamma = \frac{S_1/S_2 + \cos\beta}{\sqrt{1 + S_1^2/S_2^2 + 2S_1/S_2\cos\beta}}\,, \tag{16}$$

and

$$\cos\theta_S = \frac{S_1/S_2\cos\theta_1 + \cos\theta_2}{\sqrt{1 + S_1^2/S_2^2 + 2S_1/S_2\cos\beta}}\,, \tag{17}$$

where

$$\cos\beta = \cos\theta_1\cos\theta_2 + \sin\theta_1\sin\theta_2\cos\Delta\phi\,. \tag{18}$$

The largest flip-flop angles occurs when the two BH spins started at (or pass through) some initial configuration with $\Delta\phi = \pi/2$ as is displayed in the Fig. 16. The curves in this figure represent the probability that an equal-mass system with initial $\Delta\phi$ will have a flip-flop angle $\geq x$ given random spin orientations and spin magnitudes of the primary and secondary BHs (here labeled simply as 1 or 2). Each curve corresponds to a set of 203,401 PN evolutions ($|\alpha_1| \times |\alpha_2| \times \cos(\theta_1^0) \times \cos(\theta_2^0)$ $= 11 \times 11 \times 41 \times 41$) starting from a separation of $r = 100M$ and evolved with 3.5PN radiation reaction terms down to a separation of $5M$. The color of the curve is determined by the initial value of $\Delta\phi$.

III. UNEQUAL MASSES BINARIES

The flip-flop of BH spins in a binary system is an interesting effect since it singles out a conservative dynamical behavior that may produce important astrophysical

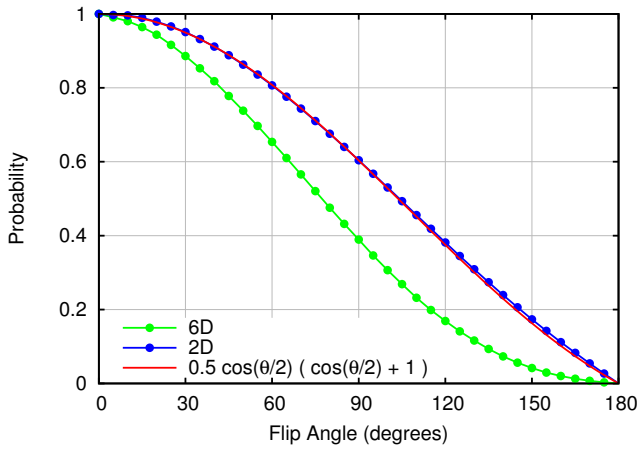

FIG. 15. The probability for the $q = 1$ case of having a flip greater than a certain angle. Distribution '2D' lets either θ_1^0 or θ_2^0 be aligned or counteraligned with $\hat{L}$ with a randomly varied cos of the other variable and spin magnitudes ratio. There are 209,450 samples that match the analytic distribution. Distribution '6D' shows the probability of flip over a generic range of spins (6 parameters) for $q = 1$, totaling 16 million evolutions.

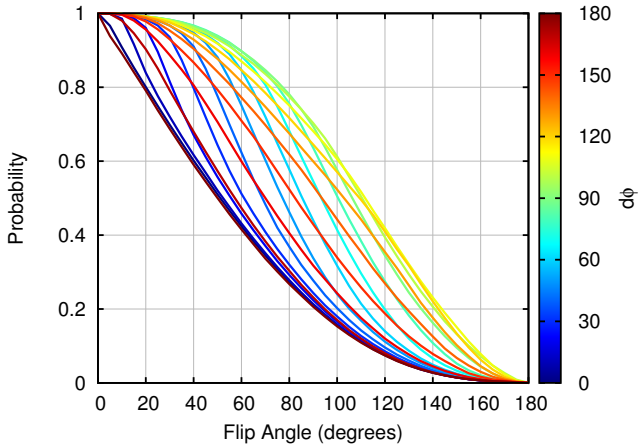

FIG. 16. The probability of a flip-flop angle $\Delta\theta_{ff} \geq x$ assuming equal masses, ($q = 1$), and a random initial spin orientations and magnitudes of both, the primary and secondary spins. Evolutions from initial separation $r = 100M$ down to $r = 5M$ are performed using 3.5PN equations of motion. The dependence with the azimuthal orientation $\Delta\phi = d\phi$ is displayed. We observe the largest flip angles probabilities for configurations with $\Delta\phi = \pi/2$ and smallest for $\Delta\phi = 0$ and π.

phenomena. In order to further evaluate the relevance to astrophysics we have to study BHBs with unequal masses and the likelihood of a given flip-angle to occur as well as the timescale (or flip-flop frequency) involved.

In the equal mass case, we have been able to discuss the geometry of the flip-flop angles in Sec. II B based on (to a good approximation) the conservation of the spin magnitudes, S_1, S_2, and S as well as the component of the total spin along the orbital angular momentum $S_{\hat{L}}$. These four conserved quantities allowed us to express the flip-flop angle in terms of the conserved quantities γ and θ_S, i.e., Eq. (6). The conservation of γ and θ_S implies that we are able to determine the flip-flop angle in terms of the initial configuration of the binary, and hence by specifying S_1/S_2, θ_1, θ_2, and $\Delta\phi$. Note that from the six variables that are needed to specify the components of the two vectors $\vec{S}_1$ and $\vec{S}_2$ only four are needed here due to the fact we compute a dimensionless flip-flop angle, hence the dependence on the ratio S_1/S_2 and the dependence on $\Delta\phi = \phi_2 - \phi_1$ appears due to the fact that for large separations a rotation of the angle ϕ is already provided by the precession of $\vec{S}$ around $\vec{L}$, spanning all orientations relative to the orbital linear momentum, $\vec{p}_i$.

In retrospective, while the flip-flop angle for equal masses can be determined geometrically, the frequency at which spins flip-flop is a dynamical quantity that requires information about the evolution of the spins as well as the orbital evolution of the BHBs. At the lowest (2PN) post-Newtonian approximation we can evaluate this frequency using the spin-evolution equations (7) assuming that the binary is separated far enough that the radial decay is negligible during a flip-flop cycle (note that the gravitational radiation frequency scales as $\sim r^{-4}$ compared to the flip-flop one scaling as $\sim r^{-3}$). The flip-flop frequency thus depends on the orbital radius r, the total spin and its projection along $\hat{L}$ as given by expression (11).

Here, in the unequal mass binary case we can assume to a certain degree of accuracy the conservation of both spin magnitudes, S_1 and S_2. $S_{\hat{L}}$ is not conserved, but the projection of the vector $\vec{S}_0$ (as given in Eq. (8)) along $\hat{L}$, denoted as $S_{0\hat{L}}$ is approximately conserved [45]. However, the total spin magnitude, S, is not conserved since the angle between the two individual spins β is no longer conserved. We will use a combination of analytic and 3.5PN numerical integrations to provide asymptotic expressions for the flip-flop angle, flip-flop frequency, and estimates of the likelihood for them to arise in astrophysical scenarios. Contemporary studies [52] could also describe the spin flips in terms of the two extreme values of the total spin.

Note that in generic binaries spin resonances of the kind studied in Refs. [53, 54] bring the azimuthal angle differences towards $\Delta\phi = 0$ and π when the spin polar orientations are significantly different, and to $\Delta\phi = \pi/2$ when they are similar [55–57]; thus allowing a further statistical reduction of the parameter space to explore.

A. Post-Newtonian Analysis

In the unequal mass binaries case the flip-flop angle will be a function of not only the intrinsic spins, $\vec{\alpha}_i = \vec{S}_i/m_i^2$, but also the radius r of the quasicircular orbit as well as the mass ratio q.

By studying the spin evolution equations (7) projected

along $\hat{L}$ (or along $\hat{J}$) we can obtain the *maximum* flip-flop angle for a given set of binary parameters, α_1, α_2, q, and r,

$$1-\cos(\Delta\theta^{ff}_{1L}) \approx \frac{2\alpha_2^2}{(1-q)^2}\left(\frac{M}{r}\right)+\frac{4\alpha_1\alpha_2^2 q}{(1-q)^3}\left(\frac{M}{r}\right)^{3/2}. \quad (19)$$

This maximum flip-flop angle of the *smaller* BH with respect to $\hat{L}$ is achieved when the smaller hole starts (or pass during its oscillation) through an anti-alignment with respect to $\hat{L}$, i.e., $\theta^0_{1L}=\pi$ and the larger BH spin $\vec{S}_2$ forms initially an angle θ^0_{2L} with $\hat{L}$ given by

$$\cos\theta^0_{2L} \approx \frac{\alpha_2}{(1-q)}\sqrt{\frac{M}{r}}+\frac{3q\alpha_1\alpha_2}{(1-q)^2}\left(\frac{M}{r}\right). \quad (20)$$

On the other hand, if we seek to maximize the flip-flop angle of the *larger* BH, we find

$$1-\cos(\Delta\theta^{ff}_{2L}) \approx \frac{2\alpha_1^2 q^2}{(1-q)^2}\left(\frac{M}{r}\right)+\frac{4\alpha_2\alpha_1^2 q^2}{(1-q)^3}\left(\frac{M}{r}\right)^{3/2}. \quad (21)$$

This maximum flip of the larger hole is achieved when the spin of this hole goes through alignment with the orbital angular momentum, i.e., $\theta^0_{2L}=0$, then the smaller BH spin forms an angle β^0_1 with $\vec{S}_2$ given by

$$\cos\theta^0_{1L} \approx \frac{q\alpha_1}{(q-1)}\sqrt{\frac{M}{r}}-\frac{3q\alpha_1\alpha_2}{(q-1)^2}\left(\frac{M}{r}\right). \quad (22)$$

In Fig. 17 we display the results of 3.5PN evolutions from $r=100M$ for 10 choices for q, 41 choices for $\cos\theta^0_1$, 41 choices for $\cos\theta^0_2$, 11 choices for $|\alpha_1|$, 11 choices for $|\alpha_2|$, and 37 choices for $\Delta\phi$ by setting $\phi^0_1=0$ and choosing different ϕ^0_2. The systems are then evolved with radiation reaction down to $5M$. The color-bar in the figures denote the initial $\Delta\phi$. The highest values happen at $\Delta\phi=\pi/2$, but the results are very insensitive on this dependence for almost every mass ratio below $q\approx 0.7$. This same property is observed in both the L- and J-frames.

We verified these analytic dependencies by performing numerical integrations of the spin evolution equations (7) for different radii, $r/M=30$, 50, 100, 150, 200, 250, and mass ratios $q=1/2$, 2/5, 1/3, 1/4, 1/5 and display a summary in Figs. 18 and 19. We compare in those plots (not fit) the analytic form of the leading flip angle (on the right-hand side of Eqs. (19) and (21)) versus the measured values as obtained from assuming the forms $1-\cos(\theta^{ff}_{1,2})=A_{L,S}/r+B_{L,S}/r^{1.5}+C_{L,S}/r^2$, and $(\Omega^{ff}_{1,2})=D_{L,S}/r+E_{L,S}/r^{1.5}+F_{L,S}/r^2$. In order to make explicit the $1\leftrightarrow 2$, $q\leftrightarrow 1/q$ symmetry of the A and D coefficients, we display the case of the larger BH flip-flop on the left of Figs. 18 and 19 in terms of $1/q>1$ variable.

The maximum angle of flip-flop with respect to J-frames is different than with respect to the L-frame due to the fact that, even during conservative evolution, the angle of precession of $\vec{L}$ around $\vec{J}$ is not preserved. In

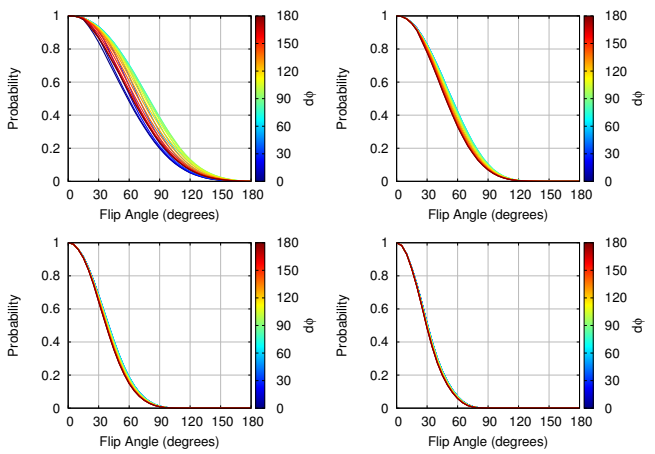

FIG. 17. The dependence of the probabilities of a flip-flop larger than a given value as a function of the initial $\Delta\phi$ angle among spins in the L-frame. Evolutions from $r=100M$ down to $r=5M$ are performed with 3.5PN including radiation reaction. From left to right and top to bottom for $q=0.9$, 0.8, 0.7, 0.6. We observe an insensitivity on $\Delta\phi$ for mass ratios of the binary below $q=0.7$. Similar results are observed in the J-frame.

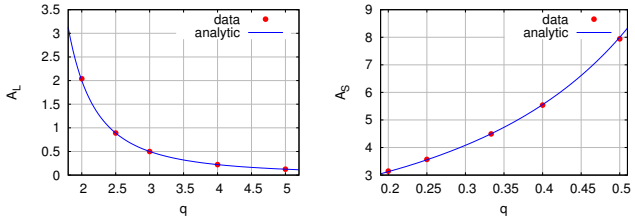

FIG. 18. Measured maximum flip-flop angle from PN evolutions versus analytic prediction (no fitting here). Here we display the leading coefficient of Eqs. (19) and (21) for the larger BH flip-flop angle (left) and smaller BH angle (right).

fact, because for unequal masses, unlike the equal mass case, the projection of the total spin $\vec{S}$ along $\vec{L}$, $S_{\hat{L}}$, is not preserved,

$$\hat{J}\cdot\hat{L}=\frac{(\ell+S_{\hat{L}})}{j}, \quad (23)$$

even if on average the magnitudes of the total angular momentum, j, and the orbital angular momentum, ℓ, are preserved.

This leads to the possibility of having larger fluctuations in the angles as "seen" in the J-frame, given by

$$1-\cos(\Delta\theta^{ff}_{1J}) \approx \frac{2\alpha_2^2}{q(1-q)^2}\left(\frac{M}{r}\right) + \frac{2\alpha_1\alpha_2^2(q-3)}{(q-1)^3}\left(\frac{M}{r}\right)^{3/2}, \quad (24)$$

and

$$1-\cos(\Delta\theta^{ff}_{2J}) \approx \frac{2\alpha_1^2 q^3}{(1-q)^2}\left(\frac{M}{r}\right)$$

$$-\frac{2\alpha_2\alpha_1^2 q^2(3q-1)}{(q-1)^3}\left(\frac{M}{r}\right)^{3/2}, \quad (25)$$

for the maximum smaller and larger BH oscillations of their spins respectively. The extreme values happen at a initial coordinate $\Delta\phi = \pi/2$ and seem to correspond to the S_{max} (and S_{min}) configurations in Fig. 2 of Ref. [58].

Note the $q \to 1/q$ symmetry of all the above expressions corresponding to a $1 \to 2$ exchange in the labels of the holes. Also at each moment of time, the conservation of S_0^L determines the angular location of the other BH given the spin of the BH with larger flip-flop angle.

The initial angle of the small hole (and between the spins) that maximizes the flip-flop as seen in the J-frame is approximated by

$$\cos\theta_{1J}^0 \approx -\frac{1}{2}\frac{(1+q)\,q\alpha_1}{(1-q)}\sqrt{\frac{M}{r}} - \frac{1}{2}\frac{(q^2+4q+1)\alpha_1\alpha_2}{(1-q)^2}\left(\frac{M}{r}\right), \quad (26)$$

for the larger BH spin initially pointing to

$$\cos\theta_{2J}^0 \approx 1 - \frac{1}{2}q^2{\alpha_1}^2\left(\frac{M}{r}\right) + q{\alpha_1}^2\alpha_2\left(\frac{M}{r}\right)^{3/2}. \quad (27)$$

While if we seek to maximize the flip-flop angle of the smaller hole as seen in the J-frame, we find

$$\cos\theta_{1J}^0 \approx -1 + \frac{1}{2}\frac{{\alpha_2}^2}{q^2}\left(\frac{M}{r}\right) + \frac{{\alpha_2}^2\alpha_1}{q}\left(\frac{M}{r}\right)^{3/2}. \quad (28)$$

In this case the spin of the larger hole points to

$$\cos\theta_{2J}^0 \approx \frac{1}{2}\frac{(1+q)\,\alpha_2}{q\,(1-q)}\sqrt{\frac{M}{r}} + \frac{1}{2}\frac{(q^2+4q+1)\alpha_2\alpha_1}{(1-q)^2}\left(\frac{M}{r}\right). \quad (29)$$

The detailed derivation is shown in Appendix A.

The frequency of the flip-flop oscillation in all these cases is given by (see Appendix A)

$$M\Omega_{1,2}^{ff} \approx \frac{3}{2}\frac{|1-q|}{(1+q)}\left(\frac{M}{r}\right)^{5/2} + 3\frac{S_1^L - S_2^L}{M^2}\left(\frac{M}{r}\right)^3 sign(1-q). \quad (30)$$

The origin of the additional term for unequal masses scaling with $\sim r^{-5/2}$ is due to the non-conservation of the angle β between the two spins (as opposed to its conservation in the $q = 1$ case). These oscillations in β are due to the differential precessional angular velocity of $\vec{S}_1$ and $\vec{S}_2$ for $q \neq 1$ and hence provides the (precessional) scaling $r^{-5/2}$.

For the sake of completeness and comparison of the time-scales involved, we give here the leading terms of the orbital frequency in a PN expansion [59]

$$M\Omega_{orb} \approx \left(\frac{M}{r}\right)^{3/2} - \frac{3+5q+3q^2}{2(1+q)^2}\left(\frac{M}{r}\right)^{5/2}$$

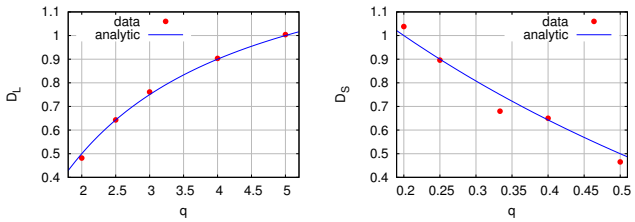

FIG. 19. Measured flip-flop frequency versus analytic prediction (no fitting here). Here we display the leading coefficient of Eq. (30) for the larger BH flip-flop angle (left) and smaller BH angle (right).

$$-\frac{2\alpha_2^L(1+4q)+q\alpha_1^L(3+2q+5q^2)}{2(1+q)^3}\left(\frac{M}{r}\right)^3 \quad (31)$$

The leading terms of the precession or azimuthal frequency are [45]

$$M\Omega_{pre} \approx \frac{7}{2}\frac{q}{(1+q)^2}\left(\frac{M}{r}\right)^{5/2} + \left[\frac{7}{2}\frac{(\alpha_1^L q^2+\alpha_2^L)}{(1+q)^2} - \frac{3}{4}\frac{(\alpha_1^L q+\alpha_2^L)}{(1+q)}\right]\left(\frac{M}{r}\right)^3 \quad (32)$$

If we now request that the flip-flop angle be exactly π in an unequal mass configuration, this might only happen for quasicircular orbits inside a critical separation r_C. In order to estimate this critical separation we may use the analytic expression for the maximum flip-flop angle of the smaller BH given in Eq. (19) and request that $\Delta\theta_{1L}^{ff} = \pi$ for total flip-flop in the L-frame. This leads to the condition

$$1 = u^2 + 2\,p\,u^3, \quad (33)$$

where

$$u = u_L = \frac{\alpha_2}{(1-q)}\sqrt{\frac{M}{r_C}}, \quad p = p^L = \frac{q\alpha_1}{\alpha_2}. \quad (34)$$

The exact solution to Eq. (33) is given by

$$u = \frac{1}{6p}\left(f^{1/3} + f^{-1/3} - 1\right), \quad (35)$$

where

$$f = \left(\sqrt{108}\sqrt{27\,p^2-1}\;p + 54\,p^2 - 1\right). \quad (36)$$

It is useful though to estimate the best scenario for large r_C, which occurs in the small to intermediate p-regime where $u \sim 1$. Thus we obtain

$$r_C \sim \frac{M\alpha_2^2}{(1-q)^2}, \quad (37)$$

with a best scenario for highly spinning BHs we get that $q > 3/4$ is needed for $r_C > 20M$. Setting up a flip of 90-degrees moves the critical radii outwards by approximately a factor two. This indicates that large flip-flop

angles, as measured in the orbital frame, are mostly expected for comparable mass binaries.

Similarly, to achieve the total flip-flop angle as seen in the J-frame, the above analysis applies with

$$u = u_J = \frac{\alpha_2}{(1-q)}\sqrt{\frac{M}{q r_C}}\,, \quad p = p^J = \frac{\alpha_1 (3-q) q^{3/2}}{2\alpha_2}\,. \tag{38}$$

This leads to similar bounds as above for comparable masses, but gets a notable increase for small mass ratios due to large precessional effects (see the bottom panel of Fig. 22).

B. Statistics

In order to evaluate the probabilities of a flip-flop angle to occur, we have performed numerical integrations of the 3.5PN equations of motion [48, 60] coupled with the spin evolution (7) for randomly varied spin magnitudes and orientations (thus representing unbiased initial conditions). This may correspond to 'dry' mergers of BHBs or to the case of 'chaotic accretion' [61]. Other scenarios involving spin alignment due to coherent accretion are possible [62] as well as the effect of resonances [53], that lead to two 'attractor' configurations, either $\Delta\phi = 0$ or $\Delta\phi = \pi$. We will study those two cases below.

We have thus performed a set of $\alpha_1 \times \cos(\theta_1^0) \times \alpha_2 \times \cos(\theta_2^0) = 20 \times 90 \times 20 \times 90 = 3,240,000$ simulations per q (we have masked the points that have one of the spins 0 or that have anti-aligned or aligned spins bringing the number for the statistics down to $2,859,120$).

Figure 20 displays the results of the probabilities (as inferred from the occurring frequency of each value) of a flip-flop angle larger than a given (by the abscissa) value to occur for each mass ratio q in the range $0.1 \leq q \leq 0.9$ (no resonances exists for the $q = 1$ case). We observe that for some values of $q > 0.7$ the probabilities for large angles can be larger than for $q \approx 1$ indicating that the leading term in Eq. (19) is preponderant as the binary inspirals down to smaller separations. This is a phenomena that we discussed in the context of maximal flip-flop at the end of Sec. III A. We thus conclude that large flip-flop angles are frequent in comparable masses binaries.

To further illustrate the probabilities of a given flip-flop angle to occur, we consider a BHB system bearing a mass ratio $q = 1/2$ at a relatively short distance, $r = 20M$. Figure 21 displays the results of a uniform initial distribution of spin magnitudes and angles.

We observe that the distribution of a given flip-flop angle has a peak at about 41° corresponding to the smaller hole flip-flop and at around 17° for the flip-flop angle of the larger hole. Flip-flop angles larger than 63° are very unlikely, in agreement with the results displayed in Fig. 20.

We mention that for unequal masses there is a difference in counting flip-flop angles in the J-frame (total angular momentum) and the L-frame (orbital angular momentum). In Fig. 22 we display the differences for a few selected mass ratios. We observe in general that larger angles are seen in the J-frame. Particularly for $q = 0.1$, due to the effects of transitional precession [63], that may reverse the orientation of $\vec{J}$. But we also observe larger angles for $q > 1/4$, configurations that exclude total transitional precession [44, 47]).

Both, the L- and J-frames are useful references to account for different astrophysical accretion scenarios.

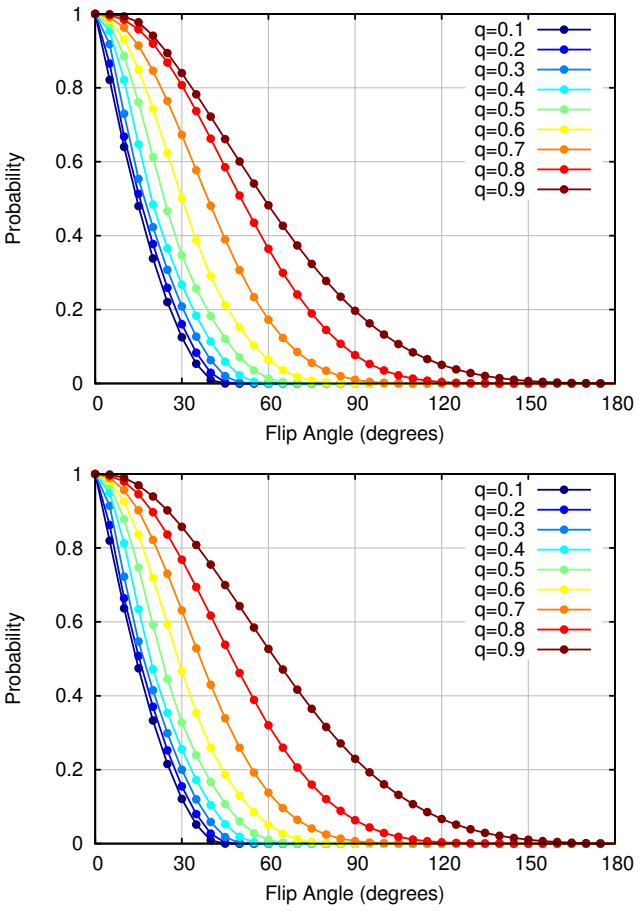

FIG. 20. The distributions of the flip angles larger than a given (abscissa) value for a binary evolved with 3.5PN from a separation $r = 100M$ to $r = 5M$ for each $0.1 \leq q \leq 0.9$ in the L-frame. The upper panel assumes an initial $\phi_1 = \phi_2$ while the lower panel assumes an initial $\phi_1 = -\phi_2$ as the resonant attractors at larger separations.

IV. CONCLUSIONS AND DISCUSSION

The unequal mass component of the flip-flop frequency, as given by Eq. (30), adds a leading term with a dependence on the orbital separation as $\sim r^{-5/2}$. This term, also proportional to $(1-q)$, eventually becomes the dominant time-scale at large enough separations. We can compare this time-scale with that for the realignment of BH spins via the Bardeen-Peterson torque effect produced by

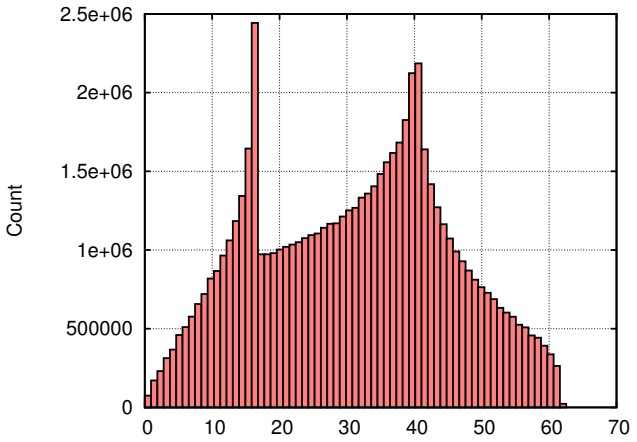

FIG. 21. The distributions of the flip angles for a binary at a constant separation $r = 20M$ and mass ratio $q = 1/2$. Spin magnitudes and angles have been chosen uniformly and the max(small, large) flip angles is evaluated. The peak at around 41° corresponds to the smaller hole spin flip. The larger hole gives an additional peak (at around 17°) towards low angles and bulks up the middle region between peaks.

accreting matter. This alignment mechanism competes with the spin flip-flop one.

The leading flip-flop period is now given by

$$T_{ff} \approx 2,000\,\mathrm{yr}\,\frac{(1+q)}{(1-q)}\left(\frac{r}{10^3 M}\right)^{5/2}\left(\frac{M}{10^8 M_\odot}\right)\,, \quad (39)$$

which is much shorter than the gravitational radiation scale [51]

$$T_{GW} \approx 1.22\times 10^6\,\mathrm{yr}\,\left(\frac{r}{10^3 M}\right)^{4}\left(\frac{M}{10^8 M_\odot}\right)\,, \quad (40)$$

and hence can take over the Bardeen-Peterson alignment mechanism [64] at an order of magnitude further separations (i.e., $10,000M$) than the gravitational radiation decay, used as reference time-scale in Ref. [65]. Thus, the flip-flop of spins shortens the time available for accretion to completely align the spins of the BH with the orbital angular momentum. However, according to Eq. (19) the angle of flip-flops gets notably reduced at large distances, hence their statistical relevance can be focused to the latest stages of merger, i.e., at closer separations or comparable mass binaries.

While in this paper we point out the relevance of studying accretion and torque exchange of matter with BHs in a *binary* system rather than on single BHs, a definitive account of these competing mechanisms should be provided by full BHB simulations in a matter filled environment that incorporates all the needed elements of a magnetohydrodynamical description of the accretion, like in Ref. [66] with spinning BHB backgrounds.

Since this flip-flop phenomena relies on the spin-spin coupling (fed by the relative spin-orbit precession in the unequal mass case), one can predict that not only BHs

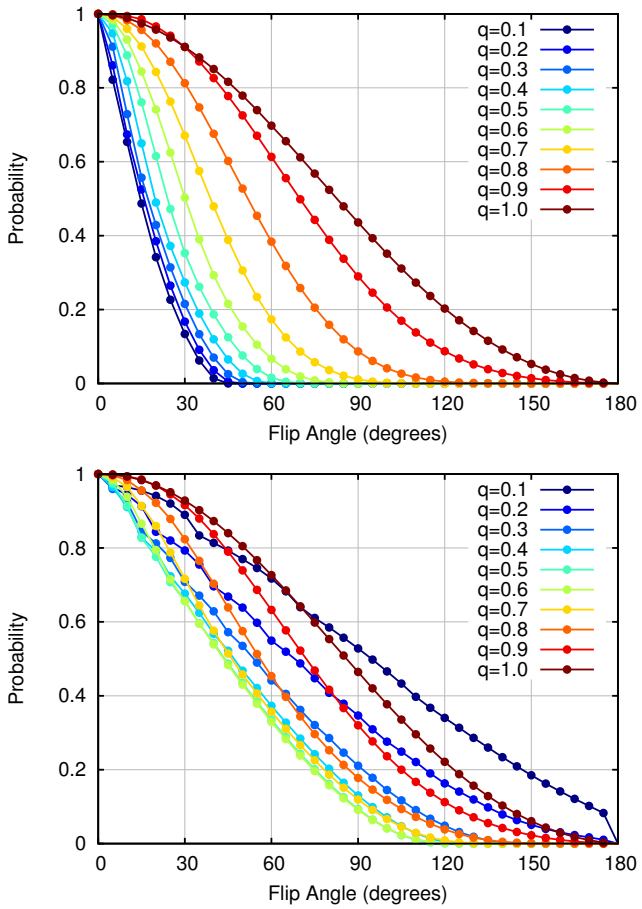

FIG. 22. Probability distribution of unequal mass flip-flops with respect to L-frame on top and with respect to J-frame below. These results are for initial random spin distributions evolved with 3.5PN form $100M$ of initial separation down to $5M$ (approximating the merger).

can see their spins flipped, but material bodies with high spin, such as neutron stars, will as well, since they have been observed to pair with comparable masses. A simple evaluation of the flip-flop frequency and angles from Eqs. (19) and (30) applied to the double pulsar PSR J0737-3039 [67] with $M = 2.587M_\odot$, $q = 0.935$, $M/r = 4.4\times 10^{-6}$, leads to a flip-flop period of $1,230$ years, i.e., the spin direction of the less massive neutron star B would change by a degree every 3.4 years. However, the total change, according to Eq. (19) will be less than a degree if the highly spinning pulsar A has an intrinsic spin $\alpha_2 < 0.25$, i.e., in order to produce observable effects nowadays its measured period should be below a millisecond instead of the actual 23 milliseconds. Notably, the spin precession frequency of pulsar B has actually been observed to be around 4.77° per year [68]. Unfortunately this precession of pulsar B meant that the highly beamed radio-emission is currently no longer pointing towards the Earth and we lost the detection of this one pulsar in 2008 [69]. Yet the spin-orbit precession of another pulsar has been measured. For the

PSR B1534+12 (a 37.9 milliseconds pulsar) a precession of 0.59° per year has been detected [70]. This underlines that other potentially observable neutron star binary systems, at closer binary separations, may lead to larger observational flip-flop effects.

ACKNOWLEDGMENTS

The authors thank M. Campanelli, J. Krolik, H. Pfeiffer and Y. Zlochower for discussions on this work. The authors gratefully acknowledge the NSF for financial support from Grants PHY-1305730, PHY-1212426, PHY-1229173, AST-1028087, PHY-0969855, OCI-0832606, and DRL-1136221. Computational resources were provided by XSEDE allocation TG-PHY060027N, and by NewHorizons and BlueSky Clusters at Rochester Institute of Technology, which were supported by NSF grant No. PHY-0722703, DMS-0820923, AST-1028087, and PHY-1229173. H.N. also acknowledges support by the Ministry of Education, Culture, Sports, Science and Technology (MEXT) Grant-in-Aid for Scientific Research on Innovative Areas, "New Developments in Astrophysics Through Multi-Messenger Observations of Gravitational Wave Sources", Grant No. 24103006.

Appendix A: Post-Newtonian Spin Evolution Equations in the L- and J- frames

We discuss the spin evolutions in Eqs. (7) by decomposing the spins along $\hat{L}$ and perpendicular to it, with unit vectors $\hat{\lambda}$ and $\hat{n}$, as shown in Fig. 12. Here, we have that this frame evolves as

$$\begin{aligned}
\dot{\hat{L}} &= \frac{2S_{\rm eff\hat{\lambda}}}{r^3}\hat{n} + \left(-\frac{2\,S_{\rm eff\hat{n}}}{r^3} + \frac{3\,\eta\,S_{0\hat{n}}\,S_{0\hat{L}}}{\ell r^3}\right)\hat{\lambda}\,,\\
\dot{\hat{n}} &= \frac{v_\lambda}{r}\hat{\lambda} - \frac{2\,S_{\rm eff\hat{\lambda}}}{r^3}\hat{L}\,,\\
\dot{\hat{\lambda}} &= -\frac{v_\lambda}{r}\hat{n} - \left(-\frac{2\,S_{\rm eff\hat{n}}}{r^3} + \frac{3\,\eta\,S_{0\hat{n}}\,S_{0\hat{L}}}{\ell r^3}\right)\hat{L}\,,
\end{aligned} \tag{A1}$$

where $\eta = q/(q+1)^2$, $\vec{S}_{\rm eff} = [1+3/(4q)]\vec{S}_1 + [1+3q/4]\vec{S}_2$, and $\vec{S}_0 = [1+1/q]\vec{S}_1 + [1+q]\vec{S}_2$. Then, we obtain the spin evolutions from Eqs. (7) as

$$\begin{aligned}
\dot{S}_{1\hat{n}} &= \Omega_1 S_{1\hat{\lambda}} - \frac{3\,S_{1\hat{L}}S_{2\hat{\lambda}}}{r^3}\left(1+\frac{q}{2}\right)\,,\\
\dot{S}_{1\hat{\lambda}} &= -\Omega_1 S_{1\hat{n}} + \frac{3\,q\,S_{1\hat{L}}S_{2\hat{n}}}{2r^3}\left(1-\frac{2\,S_{0\hat{L}}}{(1+q)\ell}\right)\\
&\quad -\frac{3S_{1\hat{L}}S_{1\hat{n}}}{q\,r^3}\left(1+\frac{q\,S_{0\hat{L}}}{(1+q)\ell}\right)\,,\\
\dot{S}_{1\hat{L}} &= \frac{3\,S_{1\hat{n}}}{2\,q\,(1+q)r^3}\Bigg[q(1+q)(2+q)S_{2\hat{\lambda}}\\
&\quad +2\left(1+q+q\frac{S_{0\hat{L}}}{\ell}\right)S_{1\hat{\lambda}}\Bigg]\\
&\quad +\frac{3\,q\,S_{2\hat{n}}\,S_{1\hat{\lambda}}}{2\,(1+q)r^3}\left[-(1+q)+2\frac{S_{0\hat{L}}}{\ell}\right]\,,
\end{aligned} \tag{A2}$$

where $S_{0\hat{L}}$ is a conserved quantity and

$$\Omega_1 = \frac{v_\lambda}{r} - \frac{\ell}{r^3}\left(2+\frac{3}{2q}\right)\left(1+\frac{S_{1\hat{L}}}{\ell}\right) + \frac{S_{2\hat{L}}}{r^3}\,, \tag{A3}$$

for $\vec{S}_1$ and similar for $\vec{S}_2$ exchanging labels 1 and 2 and $q \to 1/q$. In the above expression $S_{i\hat{L}} = \vec{S}_i\cdot\hat{L}$, $S_{i\hat{n}} = \vec{S}_i\cdot\hat{n}$, and $S_{i\hat{\lambda}} = \vec{S}_i\cdot\hat{\lambda}$; $\ell = |\vec{L}| = qM^{3/2}r^{1/2}/(1+q)^2$, and $S_{\hat{L}} = \vec{S}\cdot\hat{L}$.

1. Flip-flop frequency

The evolution of $\vec{S}_1$ and $\vec{S}_2$ along $\hat{L}$ becomes

$$\begin{aligned}
\dot{S}_{1\hat{L}} &= \frac{1}{r^3}(\vec{S}_1\times(\vec{S}+2\vec{S}_{\rm eff}))\cdot\hat{L}\\
&\quad +\frac{3}{r^3}\frac{S_{0\hat{n}}}{1+q}S_{1\hat{\lambda}}\left(1+\frac{q}{1+q}\frac{S_{0\hat{L}}}{\ell}\right)\,,\\
\dot{S}_{2\hat{L}} &= \frac{1}{r^3}(\vec{S}_2\times(\vec{S}+2\vec{S}_{\rm eff}))\cdot\hat{L}\\
&\quad +\frac{3}{r^3}\frac{qS_{0\hat{n}}}{1+q}S_{2\hat{\lambda}}\left(1+\frac{1}{1+q}\frac{S_{0\hat{L}}}{\ell}\right)\,.
\end{aligned} \tag{A4}$$

Then, the averaging over the orbital period (denoted by the brackets $\langle\rangle$) gives

$$\begin{aligned}
\langle\dot{S}_{1\hat{L}}\rangle &= \frac{3}{2r^3}(1+q)\frac{|\vec{J}|}{\ell}\left(1-\frac{q}{(1+q)^2}\frac{S_{0\hat{L}}}{\ell}\right)\\
&\quad\times(\vec{S}_1\times\vec{S}_2)\cdot\hat{J}\,,\\
\langle\dot{S}_{2\hat{L}}\rangle &= -\frac{3}{2r^3}\left(1+\frac{1}{q}\right)\frac{|\vec{J}|}{\ell}\left(1-\frac{q}{(1+q)^2}\frac{S_{0\hat{L}}}{\ell}\right)\\
&\quad\times(\vec{S}_1\times\vec{S}_2)\cdot\hat{J}\,.
\end{aligned} \tag{A5}$$

This shows the conservation of $\vec{S}_0\cdot\hat{L}$, as we have $\langle\dot{S}_{1\hat{L}}\rangle + q\langle\dot{S}_{2\hat{L}}\rangle = 0$.

On the other hand, the spin evolution projected along $\vec{J}$ can be derived from Eqs. (7) as

$$\begin{aligned}
\dot{S}_{1\hat{J}} &= = \frac{1}{r^3|\vec{J}|}\left(\left(3+\frac{3}{2q}\right)(\vec{S}_1\times\vec{S}_2)\cdot\vec{L}\right.\\
&\quad\left.+\frac{3}{1+q}\ell S_{0\hat{n}}S_{1\hat{\lambda}} + \frac{3}{1+q}S_{0\hat{n}}(\vec{S}_1\times\vec{S}_2)\cdot\hat{n}\right)\,,\\
\dot{S}_{2\hat{J}} &= = \frac{1}{r^3|\vec{J}|}\left(\left(3+\frac{3q}{2}\right)(\vec{S}_2\times\vec{S}_1)\cdot\vec{L}\right.\\
&\quad\left.+\frac{3q}{1+q}\ell S_{0\hat{n}}S_{2\hat{\lambda}} + \frac{3q}{1+q}S_{0\hat{n}}(\vec{S}_2\times\vec{S}_1)\cdot\hat{n}\right)\,,
\end{aligned} \tag{A6}$$

and then the averaging over the orbital period gives

$$\begin{aligned}
\langle\dot{S}_{1\hat{J}}\rangle &= \frac{3}{2r^3}\left(1+\frac{1}{q}\right)\left(1-\frac{q}{(1+q)^2}\frac{S_{0\hat{L}}}{\ell}\right)(\vec{S}_1\times\vec{S}_2)\cdot\hat{J}\,,\\
\langle\dot{S}_{2\hat{J}}\rangle &= -\frac{3}{2r^3}(1+q)\left(1-\frac{q}{(1+q)^2}\frac{S_{0\hat{L}}}{\ell}\right)(\vec{S}_1\times\vec{S}_2)\cdot\hat{J}\,.
\end{aligned} \tag{A7}$$

This shows the conservation of the quantity $\vec{S}_N\cdot\hat{J}$, where, $\vec{S}_N = q\vec{S}_1 + \vec{S}_2$, as we have $q\langle\dot{S}_{1\hat{J}}\rangle + \langle\dot{S}_{2\hat{J}}\rangle = 0$.

Note that the factor $\ell/(q|\vec{J}|)$ (or $q\ell/|\vec{J}|$) is different from $\langle\dot{S}_{1\hat{L}}\rangle$ (or $\langle\dot{S}_{2\hat{L}}\rangle$). This difference can be expressed as

$$\begin{aligned}\langle\dot{S}_{1\hat{J}}\rangle - \frac{\ell}{|\vec{J}|}\langle\dot{S}_{1\hat{L}}\rangle &= \frac{1}{|\vec{J}|}(\dot{\vec{S}}_1\cdot\vec{S} - \vec{S}_1\cdot\dot{\vec{L}}) \\ &= \frac{1}{|\vec{J}|}(\dot{\vec{S}}_1\cdot\vec{S}_2 - \vec{S}_1\cdot(\dot{\vec{J}} - \dot{\vec{S}}_2)) \\ &= \frac{1}{|\vec{J}|}\left[\vec{S}_1\cdot\vec{S}_2\right]^{\cdot}\,. \end{aligned} \tag{A8}$$

Therefore, the time evolution of the angle between $\vec{S}_1$ and $\vec{S}_2$ creates the different q-behavior into the two projection frames. This will affect the flip-flop angle, but not its frequency as we see below.

To obtain the flip-flop frequency (measured along $\vec{L}$ or $\vec{J}$ will be the same) we first note that

$$\begin{aligned}\dot{S}_{0\hat{L}} = &\frac{3}{2r^3}\left(\frac{1}{q} - q\right)(\vec{S}_1\times\vec{S}_2)\cdot\hat{L} \\ &+\frac{3}{r^3}\frac{S_{0\hat{n}}}{q}S_{1\hat{\lambda}}\left(1+\frac{q}{1+q}\frac{S_{0\hat{L}}}{\ell}\right) \\ &+\frac{3}{r^3}qS_{0\hat{n}}S_{2\hat{\lambda}}\left(1+\frac{1}{1+q}\frac{S_{0\hat{L}}}{\ell}\right)\,, \\ \langle\dot{S}_{0\hat{L}}\rangle = &\,0\,. \end{aligned} \tag{A9}$$

Therefore, the time dependent part of the orbital-averaged first derivative of the spins, $\langle\dot{S}_{1\hat{L}}\rangle$, $\langle\dot{S}_{2\hat{L}}\rangle$, $\langle\dot{S}_{1\hat{J}}\rangle$ and $\langle\dot{S}_{2\hat{J}}\rangle$ is only $(\vec{S}_1\times\vec{S}_2)\cdot\hat{J}$, on which we focus in the following.

The first derivative of $(\vec{S}_1\times\vec{S}_2)\cdot\hat{J}$ with respect to time can be written as

$$\begin{aligned}\frac{d}{dt}[(\vec{S}_1\times\vec{S}_2)\cdot\hat{J}] = &\frac{3}{2r^3}\frac{\ell}{|\vec{J}|}\left(1-\frac{q}{(1+q)^2}\frac{S_{0\hat{L}}}{\ell}\right) \\ &\times\left[\frac{(1-q^2)}{q}((\vec{L}\times\vec{S}_1)\times\vec{S}_2)\cdot\hat{L}\right. \\ &\left.-\left(\vec{S}_0\times(\vec{S}_1\times\vec{S}_2)\right)\cdot\hat{L}\right]. \end{aligned} \tag{A10}$$

Here, we are always using the averaged evolution equations.Taking one more time derivative of the above equation, we have

$$\begin{aligned}\frac{d^2}{dt^2}[(\vec{S}_1\times\vec{S}_2)\cdot\hat{J}] = -\Bigg[&\frac{9}{4}\frac{(1-q)^2(1+q)^2\ell^2}{q^2r^6} + \frac{9(1-q)(1+q)\ell S_{1\hat{L}}}{qr^6} - \frac{9(1-q)(1+q)\ell S_{2\hat{L}}}{qr^6} - \frac{9}{4}\frac{(3+5\,q)\,(1-q)\,{S_{1\hat{L}}}^2}{q^2r^6} \\ &+\frac{9}{2}\frac{(1-q)^2\,S_{1\hat{L}}\,S_{2\hat{L}}}{qr^6} + \frac{9}{4}\frac{(1-q)\,(5+3\,q)\,{S_{2\hat{L}}}^2}{r^6} + \frac{9}{4}\frac{(1+q)^2\left({S_1}^2 + 2\,q\,\vec{S}_1\cdot\vec{S}_2 + q^2{S_2}^2\right)}{q^2r^6} + \cdots\Bigg] \\ &\times(\vec{S}_1\times\vec{S}_2)\cdot\hat{J}\,, \end{aligned} \tag{A11}$$

where $(+\cdots)$ means higher PN order terms. This equation has the form of an harmonic oscillator (with slowly varying frequency) and reaches the two extreme positions when $\vec{S}_1$, $\vec{S}_2$, and $\vec{J}$ (or equivalently at those points $\vec{L}$) are all coplanar (and hence the triple vector product vanishes).

Therefore, we can extract a frequency as

$$\begin{aligned}\Omega_{ff}^2 = &\frac{9}{4}\frac{(1-q)^2\,M^3}{(1+q)^2\,r^5}\left(1+4\frac{M}{r}\right) + 9\,\frac{(1-q)\,(S_{1\hat{L}}-S_{2\hat{L}})M^{3/2}}{(1+q)r^{11/2}} - \frac{9}{4}\frac{(1-q)\,(3+5\,q)\,{S_{1\hat{L}}}^2}{q^2r^6} \\ &+\frac{9}{2}\frac{(1-q)^2\,S_{1\hat{L}}\,S_{2\hat{L}}}{qr^6} + \frac{9}{4}\frac{(1-q)\,(5+3\,q)\,{S_{2\hat{L}}}^2}{r^6} + \frac{9}{4}\frac{S_0^2}{r^6} + \cdots, \end{aligned} \tag{A12}$$

where we have used $\ell = (q/(1+q)^2)M^{3/2}r^{1/2}(1+2M/r)$ from Eq. (4.7) of Ref. [51], and $(+\,\cdot\,\cdot\cdot)$ stands for $O(1/r^{13/2})$ which is higher PN order corrections. Here, Ω_{ff} is constant at fixed r for $q=1$. In the unequal mass cases, this is not constant in time, but we may treat it as a constant in the flip-flop time scale because of $\dot{\Omega}_{ff}/\Omega_{ff} = O(1/r^{7/2})$.

2. Maximum flip-flop angle

The maximum flip-flop angle is calculated as follows. First, we obtain from Eq. (A11) as

$$(\vec{S}_1\times\vec{S}_2)\cdot\hat{J} = A\sin(\Omega_{ff}t)\,, \tag{A13}$$

where we have chosen the initial value by $S_{1\hat{L}}(0) = -S_1$ ($\alpha_{1\hat{L}}(0) = -\alpha_1$ where $\vec{\alpha}_i = \vec{S}_i/m_i^2$) to obtain the maximum flip-flop angle for the smaller hole. Using Eq. (A10),

the amplitude A is determined from

$$\Omega_{ff}A = \frac{3}{2r^3}\frac{\ell}{|\vec{J}|}\left(1-\frac{q}{(1+q)^2}\frac{S_{0\hat{L}}}{\ell}\right)(1+q)S_1 \qquad \text{at } t=0 \text{ as}$$

$$\times({S_2}^2 - {S_{2\hat{L}}(0)}^2)\,, \tag{A14}$$

$$A = \frac{\left({\alpha_2}^2-{\alpha_{2\hat{L}}(0)}^2\right)\alpha_1 q^2 M^{9/2}}{(1+q)^4(1-q)\sqrt{r}} + \frac{\left({\alpha_2}^2-{\alpha_{2\hat{L}}(0)}^2\right)\left(-\alpha_1 q^3+2\alpha_1 q^2+2\alpha_{2\hat{L}}(0)\,q-\alpha_{2\hat{L}}(0)\right)\alpha_1 q M^5}{(1+q)^4(1-q)^2 r}$$
$$+\frac{1}{2}\frac{\left({\alpha_2}^2-{\alpha_{2\hat{L}}(0)}^2\right)\alpha_1 M^{11/2}}{(1+q)^4(1-q)^3 r^{3/2}}(2{\alpha_1}^2q^6-6{\alpha_1}^2q^5-6\alpha_1 q^4\alpha_{2\hat{L}}(0)+6{\alpha_1}^2q^4+20\alpha_1 q^3\alpha_{2\hat{L}}(0)+8{\alpha_{2\hat{L}}(0)}^2q^2$$
$$-2{\alpha_2}^2q^2-6\alpha_1 q^2\alpha_{2\hat{L}}(0)-8q{\alpha_{2\hat{L}}(0)}^2+2{\alpha_2}^2q-{\alpha_2}^2+3{\alpha_{2\hat{L}}(0)}^2)\,, \tag{A15}$$

where $\alpha_{2\hat{L}}(0)$ is derived later. Substituting this solution into Eqs. (A5) and integrating it with respect to time, we obtain

$$\frac{\alpha_{1\hat{L}}(t)}{\alpha_1} = -1+\frac{\left({\alpha_2}^2-{\alpha_{2\hat{L}}(0)}^2\right)M}{r(1-q)^2}(1-\cos(\Omega_{ff}t)) + 2\frac{\left({\alpha_2}^2-{\alpha_{2\hat{L}}(0)}^2\right)\left(\alpha_1 q+\alpha_{2\hat{L}}(0)\right)M^{3/2}}{(1-q)^3 r^{3/2}}(1-\cos(\Omega_{ff}t))$$
$$+\frac{\left({\alpha_2}^2-{\alpha_{2\hat{L}}(0)}^2\right)\left(3{\alpha_1}^2q^2+10\alpha_1 q\alpha_{2\hat{L}}(0)-{\alpha_2}^2+4{\alpha_{2\hat{L}}(0)}^2\right)M^2}{r^2(1-q)^4}(1-\cos(\Omega_{ff}t))\,, \tag{A16}$$

with $\alpha_{1\hat{L}}(0) = -\alpha_1$. Therefore, we have the maximized flip-flop angle at $\cos(\Omega_{ff}t) = -1$, and $\alpha_{2\hat{L}}(0)$ is fixed to maximize the angle as

$$\frac{\alpha_{2\hat{L}}(0)}{\alpha_2} = \frac{\alpha_2\sqrt{M}}{(1-q)\sqrt{r}} + \frac{3q\alpha_2\alpha_1 M}{(1-q)^2 r}\,. \tag{A17}$$

Then, the solution becomes

$$\frac{\alpha_{1\hat{L}}(t)}{\alpha_1} = -1+\left[\frac{\alpha_2^2 M}{(1-q)^2 r}+\frac{2q{\alpha_2}^2\alpha_1 M^{3/2}}{(1-q)^3 r^{3/2}}\right]$$
$$\times(1-\cos(\Omega_{ff}t))\,. \tag{A18}$$

As the result, the maximum flip-flop angle becomes

$$\frac{\alpha_{1\hat{L}}(t_{\max})}{\alpha_1}+1 = 2\left[\frac{{\alpha_2}^2 M}{(1-q)^2 r}+\frac{2q{\alpha_2}^2\alpha_1 M^{3/2}}{(1-q)^3 r^{3/2}}\right]. \tag{A19}$$

Here, we need a special treatment for the $q=1$ case because of the lack of the leading term in Eq. (A12). Furthermore, since Ω_{ff} has only the leading order for $q=1$, we focus on the leading order calculation. Using the same initial configuration, $\alpha_{1\hat{L}}(0) = -\alpha_1$, the solution with the parameter $\alpha_{2\hat{L}}(0)$ is obtained as

$$\frac{\alpha_{1\hat{L}}(t)}{\alpha_1} = -\frac{\left({\alpha_2}^2-{\alpha_{2\hat{L}}(0)}^2\right)}{{\alpha_1}^2-2\alpha_1\alpha_{2\hat{L}}(0)+{\alpha_2}^2}\cos(\Omega_{ff}t)$$
$$-\frac{\left(\alpha_{2\hat{L}}(0)-\alpha_1\right)^2}{{\alpha_1}^2-2\alpha_1\alpha_{2\hat{L}}(0)+{\alpha_2}^2}\,. \tag{A20}$$

The maximum flip-flop angle is found for $\alpha_{2\hat{L}}(0) = \alpha_1$ under an assumption $\alpha_1 < \alpha_2$, and the solution becomes

$$\frac{\alpha_{1\hat{L}}(t)}{\alpha_1} = -\cos(\Omega_{ff}t)\,. \tag{A21}$$

Therefore, the maximum flip-flop angle is π.

On the other hand, in the case of $S_{2\hat{L}}(0) = S_2$ ($\alpha_{2\hat{L}}(0) = \alpha_2$), we can obtain the maximum flip-flop angle for the larger hole. The amplitude A is derived from Eq. (A10),

$$\Omega_{ff}A = \frac{3}{2qr^3}\frac{\ell}{|\vec{J}|}\left(1-\frac{q}{(1+q)^2}\frac{S_{0\hat{L}}}{\ell}\right)(1+q)S_2$$
$$\times({S_1}^2 - {S_{1\hat{L}}(0)}^2)\,. \tag{A22}$$

at $t=0$ as

$$A = \frac{\left({\alpha_1}^2-{\alpha_{1\hat{L}}(0)}^2\right)\alpha_2 q^3 M^{9/2}}{(1+q)^4(1-q)\sqrt{r}} + \frac{\left({\alpha_1}^2-{\alpha_{1\hat{L}}(0)}^2\right)\left(\alpha_{1\hat{L}}(0)\,q^3-2\alpha_{1\hat{L}}(0)\,q^2+2\alpha_2 q-\alpha_2\right)\alpha_2 q^2 M^5}{(1+q)^4(1-q)^2 r}$$
$$+\frac{1}{2}\frac{\left({\alpha_1}^2-{\alpha_{1\hat{L}}(0)}^2\right)q\alpha_2 M^{11/2}}{(1+q)^4(1-q)^3 r^{3/2}}(3{\alpha_{1\hat{L}}(0)}^2q^6-{\alpha_1}^2q^6-8{\alpha_{1\hat{L}}(0)}^2q^5+2{\alpha_1}^2q^5+6\alpha_{1\hat{L}}(0)\,q^4\alpha_2+8{\alpha_{1\hat{L}}(0)}^2q^4$$
$$-2{\alpha_1}^2q^4-20\alpha_{1\hat{L}}(0)\,q^3\alpha_2+6\alpha_{1\hat{L}}(0)\,q^2\alpha_2+6{\alpha_2}^2q^2-6{\alpha_2}^2q+2{\alpha_2}^2)\,, \tag{A23}$$

where $\alpha_{1\hat{L}}(0)$ is derived later. From a similar analysis in the above, we have

$$\frac{\alpha_{2\hat{L}}(t)}{\alpha_2} = 1-\left[\frac{q^2{\alpha_1}^2 M}{(1-q)^2 r}+\frac{2q^2{\alpha_1}^2\alpha_2 M^{3/2}}{(1-q)^3 r^{3/2}}\right]$$

$$\times(1-\cos(\Omega_{ff}t))\,, \tag{A24}$$

and

$$\frac{\alpha_{1\hat{L}}(0)}{\alpha_1} = -\frac{q\alpha_1\sqrt{M}}{(1-q)\sqrt{r}} - \frac{3q\alpha_1\alpha_2 M}{(1-q)^2 r}\,. \tag{A25}$$

Therefore, the maximum flip-flop angle is

$$1 - \frac{\alpha_{2\hat{L}}(t_{\min})}{\alpha_2} = 2\left[\frac{q^2{\alpha_1}^2 M}{(1-q)^2 r} + \frac{2q^2{\alpha_1}^2\alpha_2 M^{3/2}}{(1-q)^3 r^{3/2}}\right]. \tag{A26}$$

In the J-frame, we find the maximum flip-flop of the larger hole with $\alpha_{2\hat{L}}(0) = \alpha_2$ and a parameter $\alpha_{1\hat{L}}(0)$. The solution is

$$\begin{aligned}\frac{\alpha_{2\hat{J}}(t)}{\alpha_2} = 1 &+ \left(\frac{q^3{\alpha_1}^2 M}{(1-q)^2 r} - \frac{q^2\,(1-3\,q)\,{\alpha_1}^2\alpha_2\,M^{3/2}}{(1-q)^3\,r^{3/2}}\right)\\ &\times\cos(\Omega_{ff}t) - \frac{1}{2}\,\frac{q^2\left(q^2+1\right){\alpha_1}^2 M}{(1-q)^2\,r}\\ &-\frac{q\left(q^3+2\,q-1\right){\alpha_1}^2\alpha_2\,M^{3/2}}{(1-q)^3\,r^{3/2}}\,,\end{aligned} \tag{A27}$$

and the maximum flip-flop angle becomes

$$\begin{aligned}\frac{\alpha_{2\hat{J}}(t_{\max})}{\alpha_2} - \frac{\alpha_{2\hat{J}}(t_{\min})}{\alpha_2} = 2\Bigg[&\frac{q^3{\alpha_1}^2 M}{(1-q)^2 r}\\ &-\frac{q^2(1-3q){\alpha_1}^2\alpha_2 M^{3/2}}{(1-q)^3 r^{3/2}}\Bigg].\end{aligned} \tag{A28}$$

To obtain this flip-flop angle, the initial configuration is

$$\begin{aligned}\frac{\alpha_{2\hat{L}}(0)}{\alpha_2} &= 1\,,\\ \frac{\alpha_{2\hat{J}}(0)}{\alpha_2} &= 1 - \frac{1}{2}\,\frac{q^2{\alpha_1}^2 M}{r} + \frac{q{\alpha_1}^2\alpha_2\,M^{3/2}}{r^{3/2}}\,,\\ \frac{\alpha_{1\hat{L}}(0)}{\alpha_1} &= -\frac{1}{2}\,\frac{(3-q)\,q\alpha_1\,\sqrt{M}}{(1-q)\,\sqrt{r}}\\ &\quad+\frac{1}{2}\,\frac{(q^2-8q+1)\alpha_1\alpha_2\,M}{(1-q)^2 r}\,,\end{aligned}$$

$$\begin{aligned}\frac{\alpha_{1\hat{J}}(0)}{\alpha_1} &= -\frac{1}{2}\,\frac{(1+q)\,q\alpha_1\,\sqrt{M}}{(1-q)\,\sqrt{r}}\\ &\quad-\frac{1}{2}\,\frac{(q^2+4q+1)\alpha_1\alpha_2\,M}{(1-q)^2 r}\,.\end{aligned} \tag{A29}$$

For the smaller hole case, when we choose the initial value by $S_{1\hat{L}}(0) = -S_1$ and find $\alpha_{2\hat{L}}(0)$ to maximize the flip-flop angle that is the same ansatz as the L-frame analysis, the solution is derived as

$$\begin{aligned}\frac{\alpha_{1\hat{J}}(t)}{\alpha_1} = -1 &+ \left(-\frac{{\alpha_2}^2 M}{q\,(1-q)^2\,r} - \frac{(3-q){\alpha_2}^2\alpha_1 M^{3/2}}{(1-q)^3 r^{3/2}}\right)\\ &\times\cos(\Omega_{ff}t) + \frac{1}{2}\,\frac{\left(q^2+1\right){\alpha_2}^2 M}{q^2\,(1-q)^2\,r}\\ &-\frac{\left(q^3-2\,q-1\right){\alpha_2}^2\alpha_1\,M^{3/2}}{q\,(1-q)^3\,r^{3/2}}\,,\end{aligned} \tag{A30}$$

and the maximum flip-flop angle becomes

$$\begin{aligned}\frac{\alpha_{1\hat{J}}(t_{\max})}{\alpha_1} - \frac{\alpha_{1\hat{J}}(t_{\min})}{\alpha_1} = 2\Bigg[&\frac{{\alpha_2}^2 M}{q(1-q)^2 r}\\ &+\frac{(3-q)\alpha_2{}^2\alpha_1 M^{3/2}}{(1-q)^3 r^{3/2}}\Bigg].\end{aligned} \tag{A31}$$

The above solution is obtained for the initial configuration,

$$\begin{aligned}\frac{\alpha_{1\hat{L}}(0)}{\alpha_1} &= -1\,,\\ \frac{\alpha_{1\hat{J}}(0)}{\alpha_1} &= -1 + \frac{1}{2}\,\frac{{\alpha_2}^2 M}{q^2 r} + \frac{{\alpha_2}^2\alpha_1\,M^{3/2}}{q r^{3/2}}\,,\\ \frac{\alpha_{2\hat{L}}(0)}{\alpha_2} &= -\frac{1}{2}\,\frac{(1-3q)\,\alpha_2\,\sqrt{M}}{q\,(1-q)\,\sqrt{r}}\\ &\quad-\frac{1}{2}\,\frac{(q^2-8q+1)\alpha_2\alpha_1\,M}{(1-q)^2 r}\,,\\ \frac{\alpha_{2\hat{J}}(0)}{\alpha_2} &= \frac{1}{2}\,\frac{(1+q)\,\alpha_2\,\sqrt{M}}{q\,(1-q)\,\sqrt{r}}\\ &\quad+\frac{1}{2}\,\frac{(q^2+4q+1)\alpha_2\alpha_1\,M}{(1-q)^2 r}\,.\end{aligned} \tag{A32}$$

[1] F. Pretorius, Phys. Rev. Lett. **95**, 121101 (2005), gr-qc/0507014.

[2] M. Campanelli, C. O. Lousto, P. Marronetti, and Y. Zlochower, Phys. Rev. Lett. **96**, 111101 (2006), gr-qc/0511048.

[3] J. G. Baker, J. Centrella, D.-I. Choi, M. Koppitz, and J. van Meter, Phys. Rev. Lett. **96**, 111102 (2006), gr-qc/0511103.

[4] B. Aylott *et al.*, Class. Quant. Grav. **26**, 165008 (2009), arXiv:0901.4399 [gr-qc].

[5] B. Aylott *et al.*, Class. Quant. Grav. **26**, 114008 (2009), arXiv:0905.4227 [gr-qc].

[6] P. Ajith *et al.*, Class. Quant. Grav. **29**, 124001 (2012), arXiv:1201.5319 [gr-qc].

[7] J. Aasi *et al.* (LIGO Scientific Collaboration, Virgo Collaboration, NINJA-2 Collaboration), Class. Quant. Grav. **31**, 115004 (2014), arXiv:1401.0939 [gr-qc].

[8] M. Campanelli, C. O. Lousto, and Y. Zlochower, Phys. Rev. **D74**, 041501(R) (2006), gr-qc/0604012.

[9] M. Campanelli, C. O. Lousto, and Y. Zlochower, Phys. Rev. **D79**, 084012 (2009), arXiv:0811.3006 [gr-qc].

[10] R. Owen, Phys. Rev. **D81**, 124042 (2010), arXiv:1004.3768 [gr-qc].

[11] M. Campanelli, C. O. Lousto, Y. Zlochower, and D. Merritt, Astrophys. J. **659**, L5 (2007), gr-qc/0701164.

[12] M. Campanelli, C. O. Lousto, Y. Zlochower, and D. Merritt, Phys. Rev. Lett. **98**, 231102 (2007), gr-qc/0702133.

[13] C. O. Lousto and Y. Zlochower, Phys. Rev. Lett. **107**, 231102 (2011), arXiv:1108.2009 [gr-qc].

[14] C. O. Lousto, Y. Zlochower, M. Dotti, and M. Volonteri, Phys. Rev. **D85**, 084015 (2012), arXiv:1201.1923 [gr-qc].
[15] C. O. Lousto and Y. Zlochower, Phys. Rev. **D87**, 084027 (2013), arXiv:1211.7099 [gr-qc].
[16] S. Komossa, Adv. Astron. **2012**, 364973 (2012), arXiv:1202.1977 [astro-ph.CO].
[17] C. O. Lousto and Y. Zlochower, Phys. Rev. **D88**, 024001 (2013), arXiv:1304.3937 [gr-qc].
[18] C. O. Lousto and Y. Zlochower, Phys. Rev. Lett. **106**, 041101 (2011), arXiv:1009.0292 [gr-qc].
[19] U. Sperhake, V. Cardoso, C. D. Ott, E. Schnetter, and H. Witek, Phys. Rev. **D84**, 084038 (2011), arXiv:1105.5391 [gr-qc].
[20] C. O. Lousto and J. Healy, Phys. Rev. Lett. **114**, 141101 (2015), arXiv:1410.3830 [gr-qc].
[21] B. Szilagyi, J. Blackman, A. Buonanno, A. Taracchini, H. P. Pfeiffer, M. A. Scheel, T. Chu, L. E. Kidder, and Y. Pan, Phys. Rev. Lett. **115**, 031102 (2015), arXiv:1502.04953 [gr-qc].
[22] G. Lovelace, M. A. Scheel, R. Owen, M. Giesler, R. Katebi, B. Szilágyi, T. Chu, N. Demos, D. A. Hemberger, L. E. Kidder, H. P. Pfeiffer, and N. Afshari, Class. Quant. Grav. **32**, 065007 (2015), arXiv:1411.7297 [gr-qc].
[23] M. A. Scheel, M. Giesler, D. A. Hemberger, G. Lovelace, K. Kuper, M. Boyle, B. Szilágyi, and L. E. Kidder, Class. Quant. Grav. **32**, 105009 (2015), arXiv:1412.1803 [gr-qc].
[24] I. Ruchlin, J. Healy, C. O. Lousto, and Y. Zlochower, (2014), arXiv:1410.8607 [gr-qc].
[25] T. Bogdanović, Astrophys. Space Sci. Proc. **40**, 103 (2015), arXiv:1406.5193 [astro-ph.HE].
[26] Y. Zlochower, J. G. Baker, M. Campanelli, and C. O. Lousto, Phys. Rev. **D72**, 024021 (2005), arXiv:gr-qc/0505055.
[27] P. Marronetti, W. Tichy, B. Brügmann, J. Gonzalez, and U. Sperhake, Phys. Rev. **D77**, 064010 (2008), arXiv:0709.2160 [gr-qc].
[28] C. O. Lousto and Y. Zlochower, Phys. Rev. **D77**, 024034 (2008), arXiv:0711.1165 [gr-qc].
[29] F. Löffler, J. Faber, E. Bentivegna, T. Bode, P. Diener, R. Haas, I. Hinder, B. C. Mundim, C. D. Ott, E. Schnetter, G. Allen, M. Campanelli, and P. Laguna, Class. Quant. Grav. **29**, 115001 (2012), arXiv:1111.3344 [gr-qc].
[30] Einstein Toolkit home page: `http://einsteintoolkit.org`.
[31] Cactus Computational Toolkit home page: `http://cactuscode.org`.
[32] E. Schnetter, S. H. Hawley, and I. Hawke, Class. Quant. Grav. **21**, 1465 (2004), gr-qc/0310042.
[33] J. Thornburg, Class. Quant. Grav. **21**, 743 (2004), gr-qc/0306056.
[34] O. Dreyer, B. Krishnan, D. Shoemaker, and E. Schnetter, Phys. Rev. **D67**, 024018 (2003), gr-qc/0206008.
[35] M. Campanelli, C. O. Lousto, Y. Zlochower, B. Krishnan, and D. Merritt, Phys. Rev. **D75**, 064030 (2007), gr-qc/0612076.
[36] M. Campanelli and C. O. Lousto, Phys. Rev. **D59**, 124022 (1999), arXiv:gr-qc/9811019 [gr-qc].
[37] C. O. Lousto and Y. Zlochower, Phys. Rev. **D76**, 041502(R) (2007), gr-qc/0703061.
[38] H. Nakano, J. Healy, C. O. Lousto, and Y. Zlochower, Phys. Rev. **D91**, 104022 (2015), arXiv:1503.00718 [gr-qc].
[39] M. Campanelli, C. O. Lousto, H. Nakano, and Y. Zlochower, Phys. Rev. **D79**, 084010 (2009), arXiv:0808.0713 [gr-qc].
[40] J. Aasi *et al.* (LIGO Scientific), Class. Quant. Grav. **32**, 074001 (2015), arXiv:1411.4547 [gr-qc].
[41] H. Nakano, Class. Quant. Grav. **32**, 177002 (2015), arXiv:1501.02890 [gr-qc].
[42] A. H. Mroue, H. P. Pfeiffer, L. E. Kidder, and S. A. Teukolsky, Phys. Rev. **D82**, 124016 (2010), arXiv:1004.4697 [gr-qc].
[43] P. Peters, Phys. Rev. **136**, B1224 (1964).
[44] C. O. Lousto and Y. Zlochower, Phys. Rev. **D89**, 104052 (2014), arXiv:1312.5775 [gr-qc].
[45] E. Racine, Phys. Rev. **D78**, 044021 (2008), arXiv:0803.1820 [gr-qc].
[46] M. Campanelli, C. O. Lousto, and Y. Zlochower, Phys. Rev. **D74**, 084023 (2006), astro-ph/0608275.
[47] C. O. Lousto and Y. Zlochower, Phys. Rev. **D89**, 021501 (2014), arXiv:1307.6237 [gr-qc].
[48] A. Buonanno, Y. Chen, and T. Damour, Phys. Rev. **D74**, 104005 (2006), gr-qc/0508067.
[49] L. Blanchet, Living Rev. Rel. **17**, 2 (2014), arXiv:1310.1528 [gr-qc].
[50] G. Schäfer, AIP Conf.Proc. **1577**, 132 (2014).
[51] L. E. Kidder, Phys. Rev. **D52**, 821 (1995), gr-qc/9506022.
[52] M. Kesden, D. Gerosa, R. O'Shaughnessy, E. Berti, and U. Sperhake, Phys. Rev. Lett. **114**, 081103 (2015), arXiv:1411.0674 [gr-qc].
[53] J. D. Schnittman, Phys. Rev. **D70**, 124020 (2004), arXiv:astro-ph/0409174.
[54] T. Bogdanović, C. S. Reynolds, and M. C. Miller, Astrophys. J. **661**, L147 (2007), arXiv:astro-ph/0703054.
[55] M. Kesden, U. Sperhake, and E. Berti, Astrophys. J. **715**, 1006 (2010), arXiv:1003.4993 [astro-ph.CO].
[56] E. Berti, M. Kesden, and U. Sperhake, Phys. Rev. **D85**, 124049 (2012), arXiv:1203.2920 [astro-ph.HE].
[57] D. Gerosa, M. Kesden, E. Berti, R. O'Shaughnessy, and U. Sperhake, Phys. Rev. **D87**, 104028 (2013), arXiv:1302.4442 [gr-qc].
[58] D. Gerosa, M. Kesden, U. Sperhake, E. Berti, and R. O'Shaughnessy, Phys. Rev. **D92**, 064016 (2015), arXiv:1506.03492 [gr-qc].
[59] E. Racine, A. Buonanno, and L. E. Kidder, Phys. Rev. **D80**, 044010 (2009), arXiv:0812.4413 [gr-qc].
[60] T. Damour, P. Jaranowski, and G. Schafer, Phys. Rev. **D77**, 064032 (2008), arXiv:0711.1048 [gr-qc].
[61] A. Sesana, E. Barausse, M. Dotti, and E. M. Rossi, Astrophys. J. **794**, 104 (2014), arXiv:1402.7088 [astro-ph.CO].
[62] J. H. Krolik and J. F. Hawley, Astrophys. J. **806**, 141 (2015), arXiv:1505.01050 [astro-ph.HE].
[63] T. A. Apostolatos, C. Cutler, G. J. Sussman, and K. S. Thorne, Phys. Rev. D **49**, 6274 (1994).
[64] J. M. Bardeen and J. A. Petterson, Astrophys. J. **195**, L65 (1975).
[65] M. Coleman Miller and J. H. Krolik, Astrophys. J. **774**, 43 (2013), arXiv:1307.6569 [astro-ph.HE].
[66] S. C. Noble, B. C. Mundim, H. Nakano, J. H. Krolik, M. Campanelli, Y. Zlochower, and N. Yunes, Astrophys. J. **755**, 51 (2012), arXiv:1204.1073 [astro-ph.HE].
[67] M. Burgay, N. D'Amico, A. Possenti, R. Manchester, A. Lyne, *et al.*, Nature **426**, 531 (2003), arXiv:astro-ph/0312071 [astro-ph].

[68] R. P. Breton, V. M. Kaspi, . Kramer, Michael, M. A. McLaughlin, M. Lyutikov, *et al.*, Science **321**, 104 (2008), arXiv:0807.2644 [astro-ph].
[69] M. Burgay, (2012), arXiv:1210.0985 [astro-ph.IM].
[70] E. Fonseca, I. H. Stairs, and S. E. Thorsett, Astrophys. J. **787**, 82 (2014), arXiv:1402.4836 [astro-ph.HE].